Purdue University
Department of Physics

SEMICONDUCTOR RESEARCH
FIFTH QUARTERLY REPORT

October 1, 1961 to December 31, 1961

Contract DA 36-039-sc-87394

PURDUE RESEARCH FOUNDATION
and
UNITED STATES SIGNAL CORPS
PRF 2641

Purdue University
Department of Physics

SEMICONDUCTOR RESEARCH
FIFTH QUARTERLY REPORT

October 1, 1961 to December 31, 1961

Contract DA 36-039-sc-87394

PURDUE RESEARCH FOUNDATION
and
UNITED STATES SIGNAL CORPS
PRF 2641

PERSONNEL WORKING ON PRF 2641

October 1, 1961 - December 31, 1961

Research Staff:

H. Y. Fan, Principal Investigator
W. M. Becker*
R. Bray*
R. C. Buschert*
I. Filinski*
H. M. James
E. J. Johnson
V. A. Johnson*
W. Jung*
P. H. Keesom
R. P. Khosla*
P. H. Klose*
W. W. Lee*
K. Masumoto*
M. P. Mathur*
K. S. Mendelson*
N. Pearlman*
W. E. Pinson*
A. K. Ramdas*
L. M. Roth*
A. G. Sadasiv*
D. L. Trueblood*
J. M. van der Aa*
B. J. van der Hoeven*

Service and Clerical Staff:

V. R. Bolyard*
S. S. Leader*
M. J. Ummel*

* Paid in part or in full by PRF 2641.

TABLE OF CONTENTS

		Page
I.	ELECTRICAL AND OPTICAL PROPERTIES	
	Infrared Measurement of Hot Carrier Temperature in p-type Ge - W. Pinson and R. Bray	1
	Galvanomagnetic Properties of n-GaP - W. M. Becker and H. Y. Fan	2
	Infrared Absorption in GaSb - E. J. Johnson and H. Y. Fan	3
	Recombination Radiation in Gallium Antimonide - I. Filinski and H. Y. Fan	4
	Magnetoresistance in n-type Germanium in the Impurity Conduction Range - G. Sadasiv	4
	Cyclotron Resonance - 5mm Apparatus - T. Tohver and G. Newell	6
II.	IRRADIATION EFFECTS	
	Electron Paramagnetic Resonance-Silicon - W. Jung and G. Newell	10
	Electron Paramagnetic Resonance-Germanium - D. Trueblood and G. Newell	15
	Optical Behaviour of Irradiated Silicon - A. K. Ramdas and H. Y. Fan	17
III.	LOW TEMPERATURE STUDIES	
	Specific Heat Measurements of Indium with Small Percentages of Impurity - P. H. Keesom and B. J. L. van der Hoeven, Jr.	19
	Piezo-thermal Conductivity in Germanium - R. J. Sladek	20
	Germanium Resistance Thermometers - N. Pearlman and M. P. Mathur	20
IV.	GENERAL	
	Shallow Acceptor States in Germanium - H. M. James and K. S. Mendelson	22
	Growth of Zinc Telluride Single Crystals from the Vapour Phase - P. H. Klose	28
	Material Preparation - K. Masumoto and L. Roth	28
	TRAVEL	
	FIGURES	

I. ELECTRICAL AND OPTICAL PROPERTIES

INFRARED MEASUREMENT OF HOT CARRIER TEMPERATURE IN p-TYPE GE

W. Pinson and R. Bray

Since the last report a review and analysis of the methods and results of the infrared-hot carrier experiment have been completed, which indicated the desirability of making many modifications in the apparatus and improvements in the procedure for taking the data and analysing it. Much of the new equipment has now been designed, built and tested. The highlights of the above work will be outlined below.

The change in absorption coefficient, $\Delta \alpha$, with pulsed electric field strength will be directly determined by measuring the ratio of the pulse change in transmission, ΔI_T, due to a pulsed field, to the transmission, I_T, at zero field. The expression relating $\Delta \alpha$ to this ratio is a relatively simple one and contains all the necessary corrections for multiple reflections and the fact the light path through the sample is greater than the region subjected to high fields. The latter geometrical consideration is due to the presence of large area end contacts to eliminate injection effects at high fields. The new procedures also eliminate possible errors due to long time variations in light intensity and detector sensitivity.

However, the ratio $\Delta I_T/I_T$ cannot be measured directly because of 1) the nonlinearity of the detector, 2) the long excited carrier lifetime τ of the InSb detector ($\tau >$ pulse length), 3) lattice heating effects produced by the pulse in the Ge sample. Improved techniques and analyses for all these effects have been developed.

Our determination of the absorption coefficient α as a function of wavelength, particularly at $77^{\circ}K$, and the changes in α with lattice temperature had not been too successful for Ge with around 3×10^{15} holes/cc in the 2 to 5 micron region. The main source of the difficulty in measurement lies in the small values of α in this range (0.01 cm^{-1} to 1.0 cm^{-1}), necessitating the use of long samples with the attendant problems of uniform cooling and optical defocussing. We have, therefore, built an exchange gas cell to cool the samples, and switched to a technique of making comparative transmission measurements of our p-type sample with a pure n-type Ge sample of exactly the same length, resulting in an improvement of our measurements of α. As the several published[1,2] values of the magnitude of α disagree by 30% or more, it is necessary for us to remeasure absorption cross sections more carefully.

1. H. B. Briggs and R. C. Fletcher, Phys. Rev. 91, 1342 (1953).
2. R. Newman and W. W. Tyler, Phys. Rev. 105, 885 (1957).

GALVANOMAGNETIC PROPERTIES OF n-GaP

W. M. Becker and H. Y. Fan

Optical measurements by Edwards and Drickamer[1] indicate that the lowest conduction band in n-GaP is silicon-like, with the band minima lying along [100] directions. However, no extensive electrical measurements are available relating to this result. We have begun an investigation into the galvanomagnetic properties of this material using sulphur-doped single crystals supplied by Bell Telephone Laboratories.

Initial work showed that the usual solder or pressure contacts resulted in unsatisfactory non-ohmic high resistance contacts. Successful contact to the samples was finally made as follows: The appropriate regions of the sample surface were painted with Hanovia #38 silver paste to which a small amount of tellurium had been added. The sample was then heated in a hydrogen atmosphere at $\sim 600^{\circ}C$ for one hour, after which the silver paste was removed. Low resistance, ohmic contacts were obtained by soldering indium directly to the diffused areas.

Hall effect, conductivity, and magnetoresistance were measured on a sample having a room temperature Hall coefficient $R = -19\ cm^3/coul.$ and $\mu_H = 131\ cm^2/volt\text{-}sec.$ At $77^{\circ}K$, the Hall coefficient rises to $R = -2.2 \times 10^4\ cm^3/coul$ and $\mu_H = 333\ cm^2/volt\text{-}sec.$ Transverse magnetoresistance was observed neither at room temperature for fields up to 22,000 gauss, nor at $77^{\circ}K$ for fields up to 13,500 gauss. Based on the errors in the measurements, the room temperature value was estimated to be of the order of $\Delta\rho/\rho \sim 0.1\%$ at the highest field; the estimated value at $77^{\circ}K$ was $\Delta\rho/\rho \sim 0.1\%$. Measurements at higher fields should yield more reliable data for the determination of the magnetoresistance coefficients.

---

1. A. L. Edwards, T. E. Slykhouse, and H. G. Drickamer, J. Phys. Chem. Solids 11, 140 (1959).

INFRARED ABSORPTION IN GaSb

E. J. Johnson and H. Y. Fan

Three exciton like lines observed on the fundamental absorption edge of GaSb at 4.5°K have been described in previous progress reports[1,2]. These lines have now been observed at 1.7°K where they become sharper and more intense. The lines at 1.7°K are shown in Fig. 1. The α line is probably associated with the formation of a free exciton. A different interpretation is necessary for the β and γ lines. The possibility under consideration is that the latter lines might be due to the formation of excitons near imperfections[2]. The obvious test for this interpretation would be to look for variation in the strengths of the lines in different samples. In an attempt to verify this hypothesis, measurement was made on a sample having a somewhat smaller Hall coefficient. The result showed that the γ peak broadened into a step without appreciably increasing the strength. It is possible that the excess impurity in the sample is not of the type that gives rise to the γ peak. Preliminary measurements of the Zeeman effect have been made on the β and γ lines. The results obtained are shown in Fig. 2 and can be summarized as follows:

1. Each line splits into two components.
2. Each component occurs at higher photon energy than the line at zero magnetic field.
3. The spectra with polarization $E \parallel H$ is identical to the spectra with $E \perp H$.
4. The observed splitting is too large to be accounted for by spin.

These results need further study, but they seem to indicate effects of degenerate valence bands at $k = 0$.

---

1. E. J. Johnson and H. Y. Fan, Semiconductor Research, Third Quarterly Report, April 1, 1961 to June 30, 1961.
2. E. J. Johnson and H. Y. Fan, Semiconductor Research, Final Report, October 1, 1960 to September 30, 1961.

RECOMBINATION RADIATION IN GALLIUM ANTIMONIDE

I. Filinski and H. Y. Fan

Investigation of recombination radiation in GaSb has been continued. In the previous measurements at liquid helium temperature, there was some uncertainty regarding sample temperatures. The measurements were, therefore, repeated both at liquid nitrogen and liquid helium temperatures by actually immersing the sample in the coolant. The present results show that the position of peaks observed at liquid helium temperature for pure p-type samples are 0.752 ev $\pm$ 0.002 ev, 0.779 $\pm$ 0.02 ev, and 0.796 $\pm$ 0.02 ev. The half width of observed peaks is $\sim$ 0.006 - 0.008 ev and is larger than the resolution used viz $\sim$ 0.002 ev. The relative intensity of 0.779 ev to 0.796 ev peaks changed from sample to sample even for samples taken from different parts of the same ingot.

The following model has been considered to explain the observed emission and absorption spectra. The 0.779 ev and 0.752 ev peaks are connected with electron recombination with acceptor centers. The 0.796 ev peak is interpreted as exciton recombination at some impurity. This should be compared with the free exciton recombination expected to occur in purest samples with energy $\sim$ 0.811 ev on the basis of absorption measurements of E. J. Johnson and H. Y. Fan reported in this progress report.

MAGNETORESISTANCE IN N-TYPE GERMANIUM IN THE IMPURITY CONDUCTION RANGE

G. Sadasiv

The transverse magnetoresistance of several n-type Germanium samples has been measured in the temperature range between 4.2^{o}K and 1.2^{o}K, with magnetic fields up to 12,000 oersted. The orientation of the samples and the characteristics at room temperature and at 77.4^{o}K are given in Table I.

TABLE I

Sample	Impurity	<i>	< H >	297° K R cm^3 $coul.^{-1}$	297° K ρ ohm-cm.	77.4° K R cm^3 $coul.^{-1}$	77.4° K ρ ohm-cm.
1	Sb	001	110	10.5	.00848	13.2	.0109
2	"	001	110	44.3	.0254	70.8	.0247
3	"	011	100	57.4	.0296	92.1	.0251
4a	"	001	110	76.9	.0382	119.7	.0293
5	"	001	110	90.9	.0410	137.5	.0292
6	"	001	110	106.8	.0480	168.2	.0305
7	"	001	110		.0687		.0367
8	As	011	$0\bar{1}1$	18.9	.0144	29.3	.0204
9	"	011	$0\bar{1}1$	25.8	.0167	41.4	.0219

For samples 5 through 9, measurements were also made with the magnetic field along the < 100 > direction. There was no significant difference in the magnetoresistance.

For samples 3, 4a, 5, and 9 the resistivity ρ_H in a magnetic field H, at temperatures between 4.2°K and 1.2°K, could be described by the relation

$$\rho_H = \rho_0 \exp (\epsilon + \alpha H^2)/kT \qquad (1)$$

For sample 2, the same type of relation held for fields greater than 8000 oersted. Sample 6 showed the ϵ_2 anomaly in the resistivity[1], and in the ϵ_2 region the magnetoresistance was described by (1). The values of ρ_0, ϵ, and α are given in Table II.

TABLE II

Sample	ρ_0 ohm-cm.	ϵ ev	α ev oersted^{-2}
2	.143	$.030 \times 10^{-3}$	$.35 \times 10^{-13}$
3	.297	.113	1.27
4a	.532	.284	2.35
5	.748	.691	3.53
6	.698	1.25	4.05
9	.223	.635	1.81

In Fig. 3, the values of $\Delta\epsilon$ ($= \alpha H^2$) are plotted against H^2 for these samples.

Sample 1 had a negative magnetoresistance, reported in a previous progress report[2]. For sample 7 $\Delta \rho/\rho$ at a constant field decreased as the temperature was lowered, a behaviour similar to that observed in pure samples by Fritzsche[1].

---

1. H. Fritzsche, Phys. Rev. 99, 406 (1955).

2. G. Sadasiv, Semiconductor Research, Third Quarterly Report, April 1 to June 30, 1961.

CYCLOTRON RESONANCE-5mm APPARATUS

T. Tohver and G. Newell

Some difficulties in the design and construction of 5 mm sample cavities have been overcome. Initially, to facilitate drilling coupling holes and machining sample illumination slits, the cavity had been split into two parts. However, at 5 mm wavelengths, machining imperfections made this impractical; the split interfered with the wall currents and power was lost through the illumination window, both effects combining to lower the Q excessively. An improved design eliminates the split and the illumination window consists of a series of holes beyond cutoff (Fig. 4). The new design has been tested; it gave a cavity Q of ~ 2000 which is quite satisfactory. The variable coupling scheme shown on the accompanying sketch (Fig. 4) also works quite well - varying smoothly from zero coupling to overcoupling between the waveguide and the cavity. These results on the sample cavity and the latest performance data on 5 mm video detectors have permitted a rough estimate of the sensitivity of the equipment. These calculations are included. Also included is a schematic diagram of the microwave circuit with an indication of the sections that have been completed (Fig. 5).

Sensitivity Estimate

Optical excitation of the carriers is to be used. The sensitivity of the apparatus will be defined as the minimum number of detectable carriers. Straightforward circuit theory gives for the detected power under optimum cavity matching conditions

$$P_d = Po \times 0.193 \frac{\Delta Q^1}{Qo}$$

P_d - detected power

Po - power incident on sample cavity

ΔQ - change in cavity Q due to excited carriers

Qo - unloaded cavity Q.

Assuming the power lost to the excited carriers is small compared to the wall losses

$$\frac{\Delta Q}{Q_o} \sim \frac{Q_o}{2\omega} \frac{\int_{Sample} \sigma E^2 \, dV}{\int_{Cavity} \epsilon E^2 \, dV}$$

σ - conductivity due to excited carriers only.

For a needle-shaped sample with a diameter small compared to the wavelength and placed parallel to the maximum E-field of a TM_{110} cavity

$$\int_{Sample} \sigma E^2 \, dV \sim \sigma E_{max}^2 V_{Sample}$$

and

$$\int_{Cavity} \epsilon E^2 \, dV \sim 1/4 \, \epsilon_o E_{max}^2 V_{Cavity}$$

$$\frac{\Delta Q}{Q_o} = \frac{2Q_o}{\omega \epsilon_o} \times \frac{\sigma V_{Sample}}{V_{Cavity}}$$

Now $\sigma V_{Sample} = q (\mu_p \Delta p + u_e \Delta n) V_S$

For an order of magnitude calculation assume

$$u_e = u_p = 10^4 \frac{cm^2}{volt\text{-}sec}$$

$$= 1 \frac{m^2}{volt\text{-}sec}$$

Also call

$$V_S \times (\Delta p + \Delta n) = N$$

= Total number of carriers excited.

Take $Q_o \sim 1000$

$$\omega = 3.3 \times 10^{11} \text{ rad/sec}$$
$$e_o = 8.9 \times 10^{-12} \text{ farad/m}$$
$$q = 1.6 \times 10^{-19} \text{ coul}$$
$$V_{Cavity} \sim 100 \text{ (mm)}^3 = 10^{-7} \text{ m}^3$$
$$Po \sim 1 \text{ milliwatt}$$

Then $P_d \sim 2 \times 10^{-13}$ N watts.

At this point, the detector characteristics enter.

A crude equivalent circuit[2] for the square law detector is given below

Typically[3] $\beta = 0.13$ amps/watt

$R_o = 15$ K

Then the signal voltage is given by:

$$V_S = i_S R_o = \beta P_d Ro = 2 \times 10^{-13} N \times 0.13 \times 15 \times 10^3.$$

Thus $V_S \sim 4 \times 10^{-10}$ N volts

Assume the 1/f noise voltage across R_o at 330 c.p.s. is 100 times the thermal noise in R_o.[2]

Hence

$$V_{noise} = 100 \times (K T R_o \Delta f)^{1/2}$$

For a 30 cps bandwidth (Δf)

$$V_n \sim 4 \times 10^{-6} \text{ volts}$$

For the minimum detectable signal

$$V_{signal}^{min} = V_{noise}$$

$$V_S^{min} = 4 \times 10^{-6} \text{ v} = 4 \times 10^{-10} N^{min}$$

$$\underline{N^{min} \sim 10^4 \text{ carriers}}$$

1. G. Feher, B.S.T.J. 36, 449 (1957).
2. E. L. Ginzton, Microwave Measurements (McGraw-Hill 1957), p. 117-119.
3. Sylvania D4074 Millimeter Wave Detector (Private Communication)(B. R. Lincoln, Produce Sales Specialist).

II. IRRADIATION EFFECTS

ELECTRON PARAMAGNETIC RESONANCE - SILICON

W. Jung and G. Newell

A sample of neutron irradiated crucible grown silicon (sample #2[1], USSC No. 4, 100 Ω-cm; ORNL irradiation at T ~ 50°C, $\phi \approx 1.4 \times 10^{18}$ nvt) has been carried through an isochronal anneal in the following steps: 90° to 170°C in 10° steps for 30 minutes; 170° to 185°C in 5° steps for 30 minutes; and 200° to 500°C in 50° steps for 60 minutes each. These heat treatments were carried out in a quartz furnace in a helium atmosphere.

After each step of annealing, a complete measurement of the angular variation of the EPR spectrum at room temperature was made, using intervals of 2.5° for critical runs and 10° otherwise. The microwave Q remained high through steps 0 to 17 (400°C), indicating that the Fermi level remained in the middle of the gap, as expected from previous work. The Q decreased somewhat after step 18 (450°C), and quite appreciably after step 19 (500°C), at which point only unanalysable traces of resonance remained. The centers formed at or below 400°C are thus characteristic of intrinsic material, but the Fermi level after the 450° anneal is uncertain. A measurement of its final Fermi level is under way.

Growth and Decay Curve:

Some 12 to 14 centers are observed to grow and decay during annealing. Fig. 6 plots the concentration of those centers for which g-tensors have been worked out and which can therefore be positively identified. As discussed below, the curves for a single center are internally consistent to ± 15%, while the relative and absolute concentrations are uncertain by factors of 2 or 3 either way.

These curves clarify the relations among the previously identified centers (N, I-III) and also the relation between Oak Ridge (T ~ 50°C) and Argonne (T ~ 100°C) irradiated samples. Center I was originally observed in Argonne irradiated material containing arsenic (Sample #1[1]); it is now found in pure crucible grown material irradiated at the lower temperature and annealed at 300 to 350°C. In fact, having determined the g-tensors for centers I', V, and VI, we have now identified all the important lines in the Argonne sample and find that their relative intensities correspond roughly to the 300°C step of annealing.

A striking feature of the annealing curves shown in Fig. 6 is the occurence of pairs of centers which grow and decay together, and whose g-tensors show marked simi-

larities, as discussed later. The pairing of centers V and VI, for example, can hardly be coincidental, but no detailed explanation is yet available.

In these complicated spectra, lines overlap more often than not. Using the angular variation plots for each run, all the lines which appear (accidentally) to be in the clear at each angle are picked out for measurement, giving 15 and 40 intensity measurements for each center and temperature. These data are used to confirm the g-tensor assignments and to estimate defect concentrations. The accuracy of these estimates is discussed below.

(a) Confirmation of g-tensors: Each < 110 > type center is represented by seven branches in the angular variation plot. To verify that the branches assigned to a given center do in fact grow and decay together, separate annealing curves were constructed for each branch. For a given run the branches belonging to a single center showed a maximum spread of 2:1 in intensity, with an r.m.s. deviation of $\sim$ 16% from the mean. As several of the centers were followed over a 20:1 variation in concentration, the agreement is convincing. Taken with the very precise internal consistency criteria, this seems sufficient to confirm the g-tensor assignments. However, the possibility that pairs of g-tensors belong to a single center is mentioned below.

(b) Relative concentrations: The standard deviation of the mean intensity calculated for each center is $\pm$ 5 to 10%, and is less than the systematic variation of $\pm$ 15% seen in the curves for centers II and III below 130°C. This variation appears to result from small relative changes in the filling factors of standard and sample when the latter is replaced after each run. The annealing curve for a given center is thus self consistent to $\pm$ 15 or 20%.

Assuming similar line shapes (gaussian), the relative concentrations of two centers are given by:

$$\frac{n_1}{n_2} = \frac{A_1}{A_2} \times \left(\frac{\Delta H_1}{\Delta H_2}\right)^2,$$

where A is the amplitude and Δ H the line width. The 20% uncertainty in Δ H introduces an uncertainty of 1.4:1 in the concentrations. Further, the amplitude of the hyperfine satellites must be added to that of the principal line. This correction amounts to + 50% for Center II, but has not been applied as the h.f.s. of the other centers is as yet unknown. Relative concentrations are thus reliable only within a ratio of 2:1 unless the hyperfine structure can be assumed similar.

(c) Absolute concentrations: The absolute concentration scale is derived by comparison with the internal ruby standard using the relation

$$\frac{N_2}{V_2} = \frac{\eta_1}{\eta_2}\frac{\alpha_1}{\alpha_2}\left(\frac{\Delta H_2}{\Delta H_1}\right)^2 \cdot \frac{12A_2}{A_1} \cdot \frac{N_1}{V_2}$$

$$= 1.24 \times 10^{15} (\Delta H_2)^2 \frac{A_2}{A_1}$$

The subscripts 1 and 2 refer to ruby and the sample, respectively, while the various quantities are defined as follows:

$\frac{\eta_1}{\eta_2} = \frac{< H_{rf}^2 >_1}{< H_{rf}^2 >_2} = 0.216$

$(\frac{\alpha_1}{\alpha_2})$ = transition probability ratio ~ 4

ΔH_2 = line width of ruby = 15.9 gauss

N_1 = number of Cr^{+++} spins in the Ruby standard $\sim 2.1 \times 10^{16}$.

V_1 = sample volume = 4.12×10^{-2} cc.

$\frac{A_2}{A_1}$ = amplitude ratio

N_1 is estimated from the nominal 0.1% Cr^{+++} concentration in the ruby and may be in error by a factor of 2. Until a calibration of the standard is completed, the absolute concentrations are uncertain to a factor of 3 or 4:1.

g-tensors

The g-tensors and other properties of the centers discussed above are collected in Table 1. The tabulated values replace those given in the last report[2]; in particular, improved values for Center I have been obtained from the new data, while the N center g-tensor has been converted to absolute values consistent with the rest of the table. Center IV has not been identified with certainty in this sample, but is included for completeness. With the exception of IV, VII, and VIII, all the centers listed have been observed in at least two independent samples. Centers II, III, and N appear in floating zone material; the oxygen dependence of the others is unknown at present.

To obtain these g-tensors, a $\cos\left\{2(\theta - \theta_o')\right\}$ curve is fitted to each branch of the angular variation plot to determine adjusted values for the nine different g-values belonging to the three principal directions. Four of these values are used to

compute the g-tensor; the remainder are subjected to consistency checks. The resulting g-tensors, in general, fit the data to $\pm$ 0.5 gauss, or within half a line width. A simplified least squares treatment is being performed to improve the g-tensors; the adjustments are not expected to exceed the quoted uncertainties of .0002 in g and 0.2^{o} in θ. The g-value scale is derived from simultaneous measurements (with the same counter) of the microwave frequency and the proton precession frequency, and is free of systematic error other than that introduced by our use of the published[3] ratio

$$\frac{\mu_o}{\mu_p} = 657.4758,$$

which is valid for protons in mineral oil, whereas our proton probe uses glycerine.

Discussion:

Fig. 1 shows a striking tendancy of the damage centers to occur in pairs (II and III, V and VI, I and I', VII and VIII) which grow and anneal together. Examination of the tabulated g-tensors shows a general similarity between members of a pair; this similarity is rather more striking when the angular variation plots are examined. As this report is written we speculate that either the pairs represent two configurations of the same basic center, or that the two g-tensors actually represent the $m_s = -1 \rightarrow m_s = 0$ and $m_s = 0 \rightarrow m_s = +1$ transitions of the same S = 1 system. We have not yet had time to test these possibilities.

In addition to the centers tabulated, at least two more are present in the annealing stages near $170^{o}C$, and one or two more in the $450^{o}C$ stage. They are heavily obscured and it remains to be seen whether further analysis will disentangle them.

Several questions for future investigation are raised by these results. Foremost, perhaps, is the determination of the hyperfine structures in order to obtain information bearing on the microscopic structures. Also, however, there is the question of oxygen dependence; the rapid and complex phenomena in the $450^{o}C$ region suggest a connection with the coagulation of oxygen impurity and require more detailed investigation. We have, however, abandoned the investigation of reaction kinetics suggested in the last report: the system appears far too complex.

TABLE I

Center	~ T°C forms	~ T°C anneals	g_1 (a) ±.0002	g_2 ±.0002	g_3 ±.0002	θ ±0.2°	ΔH (b) ±0.2 g.	Impurity dependence
II	?	180°	2.0109	2.0127	1.9974	14.9°	1.2	independent
III	?	180°	2.0010	2.0072	2.0128	32°	1.2	"
N	150°	500°	2.0089	2.0125	2.0045	18.7°	1.2	"
I	250°	400°	2.0194	2.0243	1.9785	12.8°	2.4	independent or Oxygen
I'	250°	400°	1.9971	1.9942	2.0305	2.8°	2.4	
V	250°	450°	2.0125	2.0139	1.9940	4.7°	1.2	"
VI	250°	450°	2.0015	2.0041	2.0148	8.0°	1.2	"
VII	300°	500°	2.0127	2.0149	1.9937	0°	1.6	"
VIII	300°	500°	2.0017	2.0031	2.0167	0°	1.6	"
IV	400°?	500°	2.0088	2.0113	2.0050	22.0°	1.1	"

(a) g_2 is along < 1T0 >; g_1 lies in the plane containing < 001 > and < 110 >, making an angle θ with < 001 >.

(b) ΔH = full width between inflections, in gauss.

---

1. The samples used in this work are described in a previous report: Jung and Newell, Semiconductor Research, 3rd quarterly report, April 1 to June 30, 1961, p. 13.

2. Jung and Newell, Semiconductor Research, Final Report, Oct. 1, 1960 to Sept. 30, 1961, p. 10.

3. Cohen, Du Mont, et al., Rev. Mod. Phys. 27, 363 (1955).

ELECTRON PARAMAGNETIC RESONANCE - GERMANIUM

D. Trueblood and G. Newell

I. Apparatus

Construction of the x-band superheterodyne spectrometer is continuing. The microwave circuit and the klystron control circuits are complete and operate satisfactorily. Amplifiers and demodulators for the signal channel have been completed and are undergoing test.

II. Filling Factor Calculations:

As mentioned in the last report, measurements will be made on cylindrical germanium samples located on the axis of a silicon filled TE_{011} mode cylindrical cavity. The configuration is sketched in Fig. 7, which also gives calculated curves of filling factor and cavity Q as a function of sample diameter. These curves serve to determine the optimum diameter for a sample of given conductivity. They supplement the results previously given for rectangular cavities[1]. The derivation of the expressions valid for small sample diameters is sketched below.

The rf field configuration in the cavity for $r \lesssim a$ is given by:

$$E_\theta = -J_o' \left(\frac{2X_{01}\, k_{Ge} r}{D_o}\right) \sin \frac{2\pi z}{\lambda_g}$$

$$H_r = \frac{\lambda_o}{\lambda_g} J_o' \left(\frac{2X_{01}\, k_{Ge} r}{D_o}\right) \cos \frac{2\pi z}{\lambda_g},$$

$$H_z = \frac{X_{01}\, \lambda_0\, k_{Ge}}{\pi D_o} J_o \left(\frac{2X_{01}\, k_{Ge} r}{D_o}\right) \sin \frac{2\pi z}{\lambda_g},$$

and for $r \gtrsim a$ is given by:

$$E_\theta = -A_o J_o' \left[\frac{2X_{01}\, k_{si}}{D_o} \left(r + \frac{D_o}{2k_{si}} - \frac{D}{2}\right)\right] \sin \frac{2\pi z}{\lambda_g}$$

$$H_r = A_o \frac{\lambda_o}{\lambda_g} J_o' \left[\frac{2X_{01}\, k_{si}}{D_o} \left(r + \frac{D_o}{2k_{si}} - \frac{D}{2}\right)\right] \cos \frac{2\pi z}{\lambda_g}$$

$$H_z = A_o \frac{X_{01}\, \lambda_o\, k_{si}}{\pi D_o} J_o \left[\frac{2X_{01}\, k_{si}}{D_o} \left(r + \frac{D_o}{2k_{si}} - \frac{D}{2}\right)\right] \sin \frac{2\pi z}{\lambda_g}$$

where a is the radius of the Ge sample, $X_{01} = 3.832$ for a TE_{01} mode, D_o is diameter of an air filled cavity, k is the dielectric constant, A_o is an amplitude factor, λ_o is free space wavelength, λ_g is the guide wavelength, and D the loaded cavity diameter.

A_o and D were calculated as functions of a by matching $E_{tan.}$ and H across the boundary r = a. λ_g also depends on a, but for small values of a both D and λ_g approximately equal the values for a Si filled cavity.

The filling factor integral

$$n = \frac{\int_{samp.} H_{rf}^2 \, dv}{\int_{cav.} H_{rf}^2 \, dv}$$

was evaluated using the Bessel integral expression

$$\int_o^c r \left[J_n (\lambda r)\right]^2 d r = \frac{c^2}{2} \left\{\left[J_n (\lambda c)\right]^2 + \left[J_{n+1} (\lambda c)\right]^2\right\} - \frac{n c}{\lambda} J_n (\lambda c) J_{n+1} (\lambda c)$$

and the Bessel expansion to 2nd order for small a.

The result, accurate for

$$\frac{2X_{01} k a}{D_o} \lesssim 1$$

is

$$n = \frac{P + Q}{P + Q + R + S}$$

where

$$P = \left(\frac{\lambda_o}{\lambda_g}\right)^2 \left(\frac{a^2}{8}\right) \left(\frac{2X_{01} k_{Ge} a}{D_o}\right)^2$$

$$Q = \left(\frac{X_{01} \lambda_o k_{Ge}}{\pi D_o}\right)^2 \left(\frac{a^2}{2}\right) \left[1 - \frac{1}{4} \left(\frac{2X_{01} k_{Ge} a}{D_o}\right)^2\right]$$

$$R = \left(A_o \frac{\lambda_o}{\lambda_g}\right)^2 \left[\frac{D^2}{8} \left[J_2 (X_{01})\right]^2 - \frac{a^2}{8} \left(\frac{2X_{01} k_{si} a}{D_o}\right)^2\right]$$

$$S = \left(A_o \frac{X_{01} \lambda_o k_{si}}{\pi D_o}\right)^2 \left\{\frac{D^2}{8} \left[J_o (X_{01})\right]^2 - \frac{a^2}{2} \left[1 - \frac{1}{4} \left(\frac{2X_{01} k_{si} a}{D_o}\right)^2\right]\right\}$$

The equation used to estimate the loading due to Ge is

$$Q_1 = \frac{\epsilon_o \omega \int_{cav.} E_{rf}^2 \, dv}{\int_{samp.} \sigma_{Ge} E_{rf}^2 \, dv}$$

where σ_{Ge} is the Ge conductivity and is assumed independent of E so that we may remove it from the integral.. Further, σ_{Ge} is assumed small enough so as not to affect the field configuration. The calculation is similar to that of n and both results are plotted in Fig. 7. For λ_o = 3.19 cm (f = 9.4 kmc) we have D ≅ 1.20 cm. k_{si} and k_{Ge} are taken to be 11.8 and 16 respectively.

The unloaded Q of the cavity is $Q_o \cong 8700$ and Q_o and Q_1 are added in parallel to obtain the loaded Q. In view of the low conductivity of intrinsic Ge at room temp, it will be necessary to use a small sample and low temperatures to maintain a reasonable Q. The reduction in n, of course, puts a lower limit on sample radius.

---

1. Nisenoff and Fan, Semiconductor Research, Fifteenth Quarterly Report, Feb. 1, 1960 to April 30, 1960.

OPTICAL BEHAVIOUR OF IRRADIATED SILICON

A. K. Ramdas and H. Y. Fan

Our previous work[1] has shown that the two infrared absorption bands at 11.98 microns and 11.56 microns, produced in silicon by neutron or electron irradiation, are associated with the presence of oxygen in the material. The previous study of the growth of these absorption bands with 4.5 Mev electron irradiation indicated that the 11.98 micron band grew at about the same rate but saturated at a lower level with irradiation at liquid nitrogen temperature as compared with irradiation at 0^oK. Such behavior was difficult to explain on a simple basis. However, the low temperature cell used in the experiment was not suitable for accurate optical measurement, and the indication for the saturation behavior was given by only one point in the curve.

The irradiation at liquid nitrogen temperature has been repeated with a low temperature cell of better design. As was found in the previous measurement, the 11.98 micron band grew at first linearly with electron flux, at about the same rate as with 0^oK irradiation. Furthermore, the band did not saturate at a lower level as

indicated in the previous measurement but tended to saturate in the same manner as with $0^{o}K$ saturation. Thus there is no appreciable difference between the two temperatures with regard to the production of the 11.98 micron absorption band (See Fig. 8).

In agreement with the previous measurement, the 11.56 micron band was not observed during the liquid nitrogen irradiation. The band was observed after the sample had been warmed up to room temperature. Irradiation at liquid helium temperature is planned in order to ascertain whether the formation of the 11.98 micron band is inhibited at sufficiently low temperature.

---

1. A. K. Ramdas and H. Y. Fan - Semiconductor Research, First Quarterly Report, October 1, 1960 to December 31, 1960.

III. LOW TEMPERATURE STUDIES

SPECIFIC HEAT MEASUREMENTS OF INDIUM WITH SMALL PERCENTAGES OF IMPURITY

P. H. Keesom and B. J. L. van der Hoeven, Jr.

Last year Bryant and one of us[1] found that the specific heat of superconductive indium between $0.4^{\circ}K$ and $0.7^{\circ}K$ was less than the lattice contribution in the normal state.

Ferrel[2] proposed an explanation of this specific heat anomaly which is based on an anomalous dispersion in the phonon spectrum. The interaction between phonons and electrons leads to a self energy of the phonons, due to creation and reabsorption of electron-hole pairs. The energy gap in the electronic states of the superconductor prevents the creation of electron-hole pairs for phonons with too small an energy, and, consequently, the self energy term disappears for a certain range of phonon frequencies. This leads to a lowering of the frequencies of the phonons in the superconductive state, relative to the phonons in the normal state. As a consequence, a new term, equal to $-BT^2$, is obtained in the specific heat of the superconductor.

A distinct advantage of this theory is that it predicts the effect for indium, but not for tin, since it depends on the coupling between phonons and electrons.

As one of the experimental tests, Ferrell indicates that for phonons with wavelengths longer than the coherence length, this effect should disappear. The coherence length is a measure of the extension of the electron wave packet taking part in the superconductive phenomena. His idea is that for phonon wavelengths longer than the coherence length, we expect the normal bulk elastic constants to give a correct description of the sound waves, and thus, also the normal lattice specific heat. From the work of Pippard[3], Ferrell deduces that if a metal (such as indium) showing the heat anomaly were heavily enough doped with an alloying impurity to reduce significantly the coherence length, then the anomaly would disappear.

Measurements on indium doped with tin are now in progress.

---

1. C. A. Bryant and P. H. Keesom, Phys. Rev. 123, No. 2, 491 (1961).
2. R. A. Ferrell, Phys. Rev. letters 6, No. 10, 541 (1961).
3. A. B. Pippard, Phil. Mag. 46, 1104 (1955).

PIEZO-THERMAL CONDUCTIVITY IN GERMANIUM

R. J. Sladek

The thermal conductivity of degenerate n-type germanium (containing 2×10^{17} Sb atoms/cc) has been measured between $1.5^{\circ}K$ and $4.1^{\circ}K$ with tensile stresses from zero to 1.5×10^{8} dynes/cm^2 applied in the [110] crystallographic direction. Fig. 9 shows the temperature dependence of the thermal conductivity with no applied stress and with 1.0×10^{8} dynes/cm^2 applied. For all temperatures, this applied stress increases the thermal conductivity only slightly (about 10%). This is in sharp contrast to the behavior of germanium more lightly doped with Sb for which large increases in the thermal conductivity can be obtained at the lower temperatures[1]. A detailed comparison of these effects is given in Fig. 10 which shows that the ratio of unstressed to stressed thermal conductivity is independent of temperature for the degenerate sample while this ratio decreases strongly with decreasing temperature for the more lightly doped sample (data on the latter from reference 1).

The relatively small piezo-thermal conductivity effect in the degenerate sample can be explained qualitatively by noting that in such a sample the donor levels have merged with the conduction band and the donors are ionized even at the lowest temperatures. Consequently, the strongly stress-dependent scattering of phonons by bound donor electrons[1] is absent.

The different temperature dependences of the piezo-thermal conductivity for the degenerate and non-degenerate samples also suggest that the mechanisms by which electrons scatter phonons are different in these two types of materials.

---

1. R. W. Keyes and R. J. Sladek, Phys. Rev. (Jan. 15, 1962).

GERMANIUM RESISTANCE THERMOMETERS

N. Pearlman and M. P. Mathur

In the measurements described in earlier Progress Reports, it was found that the reproducibility of the thermometers in successive runs was rather good, provided that relative values $R(T)/R_o$ were compared, where R_o is the resistance at an arbitrary temperature (usually $R_o = R(4^{\circ}K)$). However, $R(T)$ itself was usually reproducible only to such an extent that a given resistance value might correspond, on different runs, to temperatures differing by as much as $\Delta T \sim 0.1^{\circ}K$.

Part of these differences could be accounted for, on runs between which leads had been resoldered to the thermometer, by the possibility that melting of the solder attaching the heavy leads to the thermometer had changed the effective sample dimensions between leads. To avoid this, the heavy leads were attached to the thermometer with tin-lead solder while the thin wires were attached to the heavy leads with low-melting cerroseal solder.

Another possible factor affecting reproducibility could be strain in the thermometer due to differential thermal contraction between the thermometer and the base on which it is mounted, or the adhesive bonding it to the base. The former is apparently not too important, since thermometers mounted on a Ge base did not behave differently from those measured earlier, mounted on a copper base. In order to eliminate the latter influence thermometers were made in the "L" shape shown in Fig. 11 and mounted on the short leg. With this configuration, reproducibility on successive runs becomes a few millidegrees. The thermal contact resistance dT/dP between thermometer and base, where P is power dissipated in the thermometer, is about the same as that for the earlier thermometers, roughly a millidegree per microwatt, which is about two orders of magnitude smaller than that reported for encapsulated Ge thermometers by Lindenfeld[1].

---

1. P. Lindenfeld, Rev. Sci. Inst. 32, 9 (1961).

IV. GENERAL

SHALLOW ACCEPTOR STATES IN GERMANIUM

H. M. James and K. S. Mendelson

Solutions of the effective mass equations for shallow acceptors in germanium have been obtained using a variational method in which the angular dependence of the trial function was determined from symmetry considerations[1] and the radial dependence was determined by the variational calculation.

Let J_x, J_y, J_z be matrices corresponding to components of angular momentum 3/2. Let

$$\{J_\alpha J_\beta\} = \frac{1}{2}\left(J_\alpha J_\beta + J_\beta J_\alpha\right).$$

Then the effective mass Hamiltonian for acceptors in germanium can be written

$$H = -\frac{\hbar^2}{2m}\left(\gamma_1 + \frac{5}{2}\gamma_2\right)\nabla^2 + \frac{\hbar^2}{m}\gamma_2\left(J_x^2\frac{\partial^2}{\partial x^2} + J_y^2\frac{\partial^2}{\partial y^2} + J_z^2\frac{\partial^2}{\partial z^2}\right) + \frac{2\hbar^2}{m}\gamma_3\left[\{J_x J_y\}\frac{\partial^2}{\partial x\partial y} + \{J_y J_z\}\frac{\partial^2}{\partial y\partial z} + \{J_z J_x\}\frac{\partial^2}{\partial z\partial x}\right] - \frac{e^2}{Kr}. \quad (1)$$

where γ_1, γ_2, γ_3 are constants which can be determined from cyclotron resonance experiments[2,3]. The energy has been chosen to be positive in the direction of increasing hole energy; thus the bound state energies of the acceptor will be negative.

The ground state wave functions transform according to the Γ_8 irreducible representation of the double tetrahedral group. The function

$$\psi = \begin{bmatrix}1\\0\\0\\0\end{bmatrix} f_1(r) + \begin{bmatrix}z^2 - \frac{1}{2}(x^2+y^2)\\0\\-\frac{3}{2}(x^2-y^2)\\0\end{bmatrix} f_2(r) + i\begin{bmatrix}0\\z(x+iy)\\0\\xy\end{bmatrix} f_3(r), \quad (2)$$

having this transformation property, was used as a trial function[1]. The first term has s-like dependence on angle, and the others have d-like dependence. (Factors of r^2 were included in the d-like angular terms for convenience in calculation.) Extremalizing the functional

$$L = \int \psi^* (H - E) \psi \, d^3x$$

with respect to variations of the f's leads to a system of ordinary differential equations for the f's. It is convenient to define

$$g_1 = r f_1,$$
$$g_2 = r^3 f_2,$$
$$g_3 = r^3 f_3.$$

The differential equations for the g's are then

$$g_1'' + (\epsilon + \frac{2}{r}) g_1 - \frac{4\gamma_2}{5\gamma_1} (g_2'' + \frac{3}{r} g_2') + \frac{2\sqrt{3}\,\gamma_3}{5\gamma_1} (g_3'' + \frac{3}{r} g_3') = 0, \qquad (3a)$$

$$-\frac{2\gamma_2}{\gamma_1} (g_1'' - \frac{3}{r} g_1' + \frac{3}{r^2} g_1) + g_2'' + (\epsilon + \frac{2}{r} - \frac{6}{r^2}) g_2 = 0, \qquad (3b)$$

$$\frac{2\sqrt{3}\,\gamma_3}{\gamma_1} (g_1'' - \frac{3}{r} g_1' + \frac{3}{r^2} g_1) + g_3'' + (\epsilon + \frac{2}{r} - \frac{6}{r^2}) g_3 = 0, \qquad (3c)$$

Here we have used as units of energy and length

$$\epsilon_o = \frac{m e^4}{2 K^2 h^2 \gamma_1} = 0.00403 \text{ ev},$$
$$L_o = \frac{K h^2 \gamma_1}{m e^2} = 110 \text{ Å}.$$

The functions g_i must satisfy the boundary conditions

$$g_i \to 0 \text{ as } r \to 0, \; r \to \infty \quad (i = 1, 2, 3).$$

We first observe that these equations have solutions with $g_1 \equiv 0$ and g_2, g_3 satisfying

$$g_2'' + (\epsilon + \frac{2}{r} - \frac{6}{r^2}) g_2 = 0,$$
$$g_3 = \frac{2\gamma_2}{\sqrt{3}\,\gamma_3} g_2.$$

This equation for g_2 is simply the equation for hydrogenic radial functions with $\ell = 2$. It will have acceptable solutions for $\epsilon = -1/n^2$, $n = 3, 4, 5, \ldots$ These solutions, however, do not give an approximation to the ground state function. The lowest energy, $\epsilon = -1/9$, $E = -0.00045$ ev, is much higher than the experimental ground state energies[4] of -0.010 to -0.014 ev.

If $g_1 \not\equiv 0$, we can eliminate it from Eqs. (3a) and (3b). This gives

$$\frac{d^2}{dr^2}\left(\sqrt{3}\,\gamma_3\, g_2 + \gamma_2\, g_3\right) + \left(\epsilon + \frac{2}{r} - \frac{6}{r^2}\right)\left(\sqrt{3}\,\gamma_3\, g_2 + \gamma_2\, g_3\right) = 0.$$

This is again the hydrogenic radial equation. There will be acceptable, non-trivial solutions for $\sqrt{3}\,\gamma_3\, g_2 + \gamma_2\, g_3$ only when $\epsilon = -1/n^2$. As we have seen, these solutions will not be approximations to the ground state functions. Thus for the ground state we must have

$$g_3 = -\frac{\sqrt{3}\,\gamma_3}{\gamma_2}\, g_2.$$

Elimination of g_3 from Eqs. (3) gives

$$g_1'' + \left(\epsilon + \frac{2}{r}\right) g_1 - A\left(g_2'' + \frac{3}{r}\, g_2'\right) = 0, \tag{4a}$$

$$-B\left(g_1'' - \frac{3}{r}\, g_1' + \frac{3}{r^2}\, g_1\right) + g_2'' + \left(\epsilon + \frac{2}{r} - \frac{6}{r^2}\right) g_2 = 0, \tag{4b}$$

where

$$A = \frac{2\left(2\gamma_2^{\,2} + 3\gamma_3^{\,2}\right)}{5\,\gamma_1\,\gamma_2},$$

$$B = \frac{2\gamma_2}{\gamma_1}.$$

These equations cannot be solved analytically. We have therefore obtained numerical solutions using the Runge-Kutta method[5].

To determine the initial conditions, one can try solutions of the form

$$\begin{aligned} g_1 &= r^{n_1} \sum_{\tau=0}^{\infty} a_\tau\, r^\tau, \\ g_2 &= r^{n_2} \sum_{\tau=0}^{\infty} b_\tau\, r^\tau. \end{aligned} \tag{5}$$

One finds that $n_1 = n_2 = n = 3, 1, 0, -2$. We note that the indices differ by integers. In this case, there will not be a solution of the form (5) for each value of n[6]. There will be a solution of the form (5) for $n = 3$. We denote this solution by

$$y_1 = r^3 \sum_{\tau=0}^{\infty} a_\tau r^\tau$$
$$y_2 = r^3 \sum_{\tau=0}^{\infty} b_\tau r^\tau \qquad (6)$$

In addition there will be a solution of the form[6]

$$z_1 = y_1 \ln r + \bar{g}_1$$
$$z_2 = y_2 \ln r + \bar{g}_2$$

We denote this solution by

$$z_1 = y_1 \ln r + r \sum_{\tau=0}^{\infty} c_\tau r^\tau,$$
$$z_2 = y_2 \ln r + r^2 \sum_{\tau=0}^{\infty} d_\tau r^\tau. \qquad (7)$$

From the differential equations, one can derive recurrence relations for the coefficients a_τ, b_τ, c_τ, d_τ. There are two other linearly independent solutions of Eq. (4), but they do not behave acceptably as $r \to 0$.

It is also necessary to consider the asymptotic behavior as $r \to \infty$. There are four linearly independent asymptotic solutions that have the forms

$$g_1 \sim a e^{\pm \alpha r}, \qquad g_2 \sim b e^{\pm \alpha r}$$
or $\qquad (\alpha > \beta) \qquad (8)$
$$g_1 \sim a e^{\pm \beta r} \qquad g_2 \sim -b e^{\pm \beta r}.$$

As $r \to \infty$, the solution with $e^{\alpha r}$ will blow up more rapidly than that with $e^{\beta r}$; hence this will be called the dominant solution, and that with $e^{\beta r}$ the sub-dominant solution.

For a given energy, one can use the solutions described by Eqs. (6) or (7), or any linear combinations of them, to determine $g_1(r_o)$, $g'_1(r_o)$, $g_2(r_o)$, $g'_2(r_o)$

(r_o small) for a solution that is well-behaved as $r \to 0$. Starting from r_o with these initial values, one can integrate Eq. (4) numerically to obtain a solution that is well-behaved at the origin but will, in general, become infinite as $r \to \infty$. If an arbitrary linear combination of Eqs. (6) and (7) is used to obtain the initial conditions, the solution at large r will approach some linear combination of the dominant and sub-dominant solutions. In general, such a solution will blow up even if ϵ is an eigenvalue of the problem. To obtain a solution that is well-behaved as $r \to \infty$, it is necessary to adjust not only the energy, but also the linear combination of Eqs. (6) and (7) that is used to obtain the initial conditions.

One can, for any ϵ, choose the initial conditions so that only the sub-dominant term appears at large r. For an energy that is an eigenvalue, the sub-dominant term disappears also, and one obtains a solution that is well-behaved as $r \to \infty$. To eliminate the dominant solution, the following procedure was used. For each energy two solutions (g_1, g_2) were determined, starting from initial conditions determined by Eqs. (6) and (7), respectively. It was found that the solution given by Eq. (6) had essentially pure dominant behavior at large r. We took the ratio g_1/g_2 of this solution at large r to be a/b (Eq. (8)). Using the value of a/b obtained in this way, we chose a linear combination of the solutions such that the ratio g_1/g_2 at the end of the range of integration (determined by practical considerations of computing time) was -a/b. The resulting curves gave essentially pure sub-dominant behavior at large r. The value of g_1 at a point near the end of the range of integration, chosen so far out that a well-behaved solution would be negligible, was used as a measure of the amount of sub-dominant solution present. By repeating this process for several energies, it was possible to find eigenvalues and corresponding eigenfunctions.

Using this method, we determined the energy and radial functions for the ground state, and for the first excited state described by the trial function (2). We also applied a similar method to the Γ_7 and Γ_6 excited states[1]. For the Γ_7 states, we used the trial function

$$\psi = \begin{bmatrix} x + iy \\ 0 \\ -3\,(x - iy) \\ 2\,iz \end{bmatrix} f_1(r) + \begin{bmatrix} -\frac{3}{4}\left[(z^2 - \frac{1}{5}r^2)(x + iy) + (x - iy)^3\right] \\ \frac{i\,3}{2}\left[z(x + iy)^2 + z(x - iy)^2\right] \\ -\frac{3}{4}\left[7(z^2 - \frac{1}{5}r^2)(x - iy) - (x + iy)^3\right] \\ -3rz\,(z^2 - \frac{3}{5}r^2) \end{bmatrix} f_2(r)$$

and for the Γ_6 states we used the trial function

$$\psi = \begin{bmatrix} 3\,(x - iy) \\ 2\,iz \\ x + iy \\ 0 \end{bmatrix} f_1(r) + \begin{bmatrix} -\frac{3}{4}\left[7\left(z^2 - \frac{1}{5}r^2\right)(x - iy) - (x + iy)^3\right] \\ 3iz\,(s^2 - \frac{3}{5}r^2) \\ \frac{3}{4}\left[\left(z^2 - \frac{1}{5}r^2\right)(x + iy) + (x - iy)^3\right] \\ \frac{i\sqrt{3}}{2}\left[z(x + iy)^2 + z(x - iy)^2\right] \end{bmatrix} f_2(r)$$

Here there are only two terms in each trial function, and the variational procedure gave immeadiately two coupled differential equations for the f's. These equations were solved numerically by the method described above. The energies thus found are shown in Table I, and the radial functions in Figs. 12 - 16. These results were obtained using the values of γ_1, γ_2, γ_3 given in reference 3.

TABLE I. Eigenvalues of Effective Mass Hamiltonian for Shallow Acceptor States in Germanium.

Trial Function	Energy	
	ϵ_0	10^{-3} ev
Γ_8	-2.32	-9.28
	-0.690	-2.76
Γ_7	-0.484	-1.94
	-0.250	-1.00
Γ_6	-0.146	-0.584

1. D. Schechter, Theory of Shallow Acceptor States in Silicon and Germanium. Ph.D. Thesis, Carnegie Institute of Technology, unpublished.
2. G. Dresselhaus, A. F. Kip, and C. Kittel, Phys. Rev. 98, 368 (1955).
3. B. W. Levinger and D. R. Frankl, J. Phys. Chem. Solids, 20, 281 (1961).
4. P. Fisher and H. Y. Fan, Phys. Rev. Letters 2, 456 (1959).
5. F. B. Hildebrand, "Introduction to Numerical Analysis" (McGraw Hill, New York, 1956) pp. 233-239.
6. E. L. Ince, "Ordinary Differential Equations" (Dover Publications Inc., New York, 1956) p. 160 and Sec. 15.311.

GROWTH OF ZINC TELLURIDE SINGLE CRYSTALS FROM THE VAPOUR PHASE

P. H. Klose

Work has been started to prepare the compound semiconductor zinc telluride, ZnTe. Equimolecular parts of the chemically pure constituents are weighed, mechanically mixed, and melted together in a quartz tube. A purified hydrogen ambient is used to prevent oxidation during this process. Any excess metal is distilled away afterwards in a high vacuum furnace. The material so prepared is already quite dense and is in the shape of a rod. This rod is then placed in a furnace for the growing of the crystal. The furnace is essentially similar to that described by Polich and co-workers[1]. Experiments are being carried out to determine the optimum temperature profile of the growing furnace and the corresponding rate of growth in order to obtain single crystals. Measurements of Hall coefficient and resistivity of the material prepared have been made at room temperature. Hall mobilities of 50 cm^2/volt-sec have been found for samples with resistivities of the order of 1 Ω cm.

---

1. Piper, Polich, J. A. P., 32, 1278 (1961).

MATERIAL PREPARATION

K. Masumoto and L. Roth

Work has continued on the preparation of large crystals of ZnSb under various growth conditions using the Bridgman method. Attempts were made to obtain single crystals by the Czochralski technique using the Bridgman method crystals as seeds. So far, it has not been possible to obtain large single crystals without twinning. Improvements are being made in the crystal pulling apparatus with the aim of obtaining single crystals.

The usual work of making single crystals of Ge, InSb, and GaSb continues.

TRAVEL ON PRF 2641

October 1, 1961 - December 31, 1961

Dr. Ralph Bray - Chicago, Illinois
October 9, 1961
To visit the Electronic Equipment Display at the National Electronics Conference.

Dr. R. C. Buschert - Chicago, Illinois
October 9, 1961
To visit the Electronic Equipment Display at the National Electronics Conference.

Dr. W. M. Becker - Chicago, Illinois
October 9, 1961
To visit the Electronic Equipment Display at the National Electronics Conference

Dr. R. J. Sladek - Argonne, Illinois
October 20-21, 1961
To attend the Midwest Solid State Conference at Argonne National Laboratory and present a paper.

Dr. Ralph Bray - Argonne, Illinois
October 20-21, 1961
To attend the Midwest Solid State Conference at Argonne National Laboratory and present a paper.

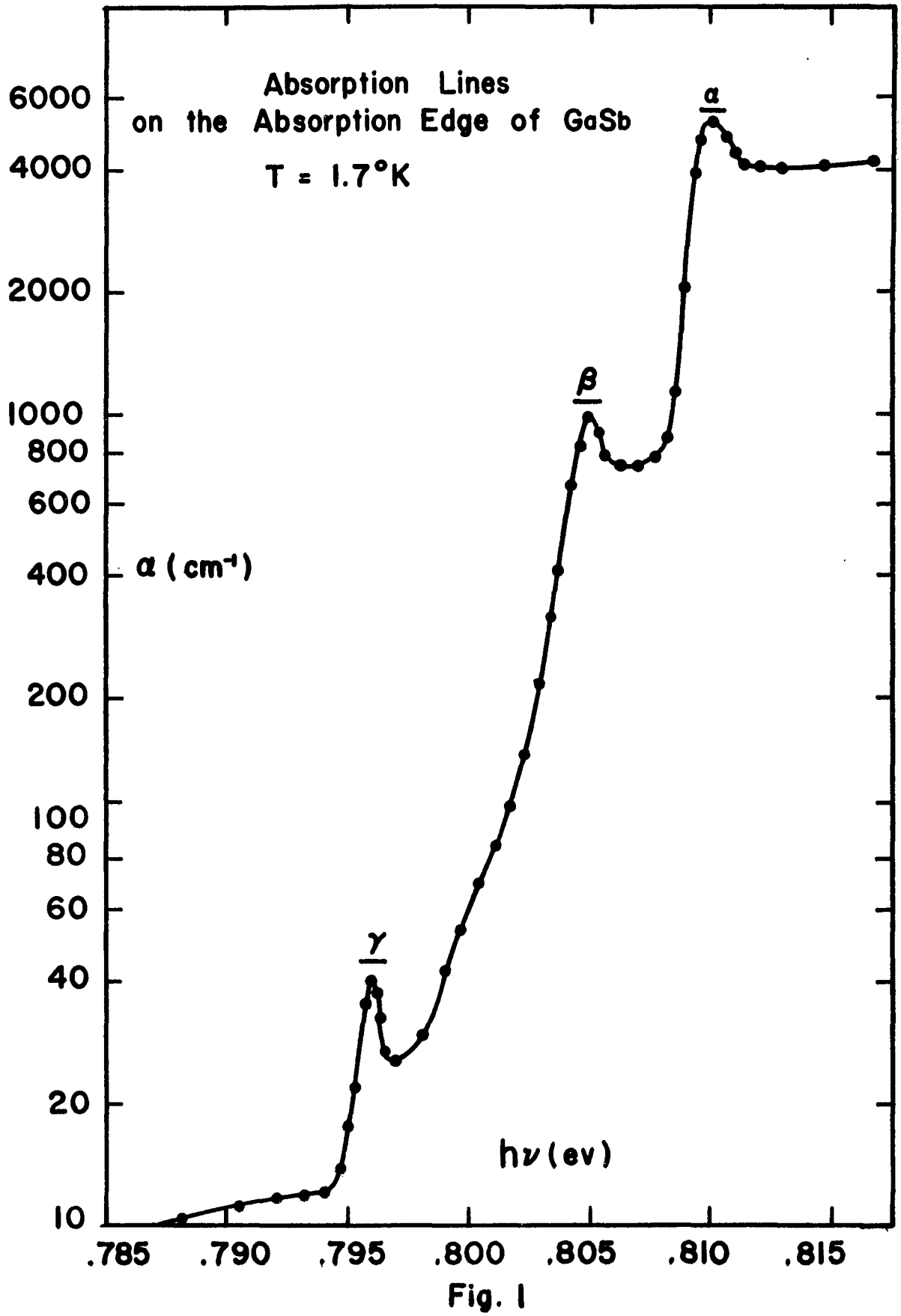
Absorption Lines
on the Absorption Edge of GaSb
T = 1.7°K
α
β
γ
6000
4000
2000
1000
800
600
400
200
100
80
60
40
20
10
α (cm⁻¹)
hν (ev)
.785
.790
.795
.800
.805
.810
.815

Fig. 1

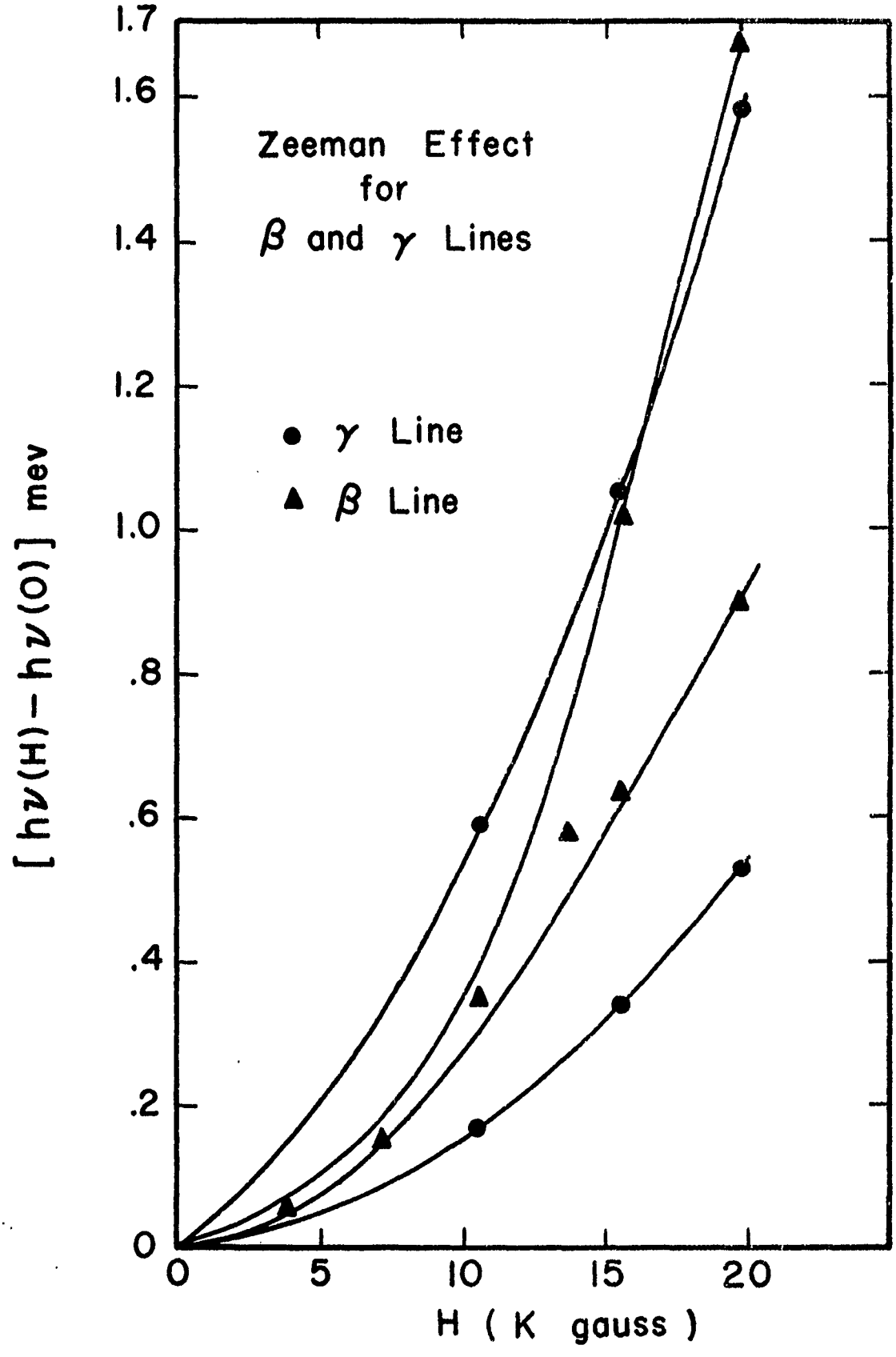
Zeeman Effect
for
β and γ Lines
γ Line
β Line
[hν(H) − hν(0)] mev
H (K gauss)
0
.2
.4
.6
.8
1.0
1.2
1.4
1.6
1.7
0
5
10
15
20

Fig. 2

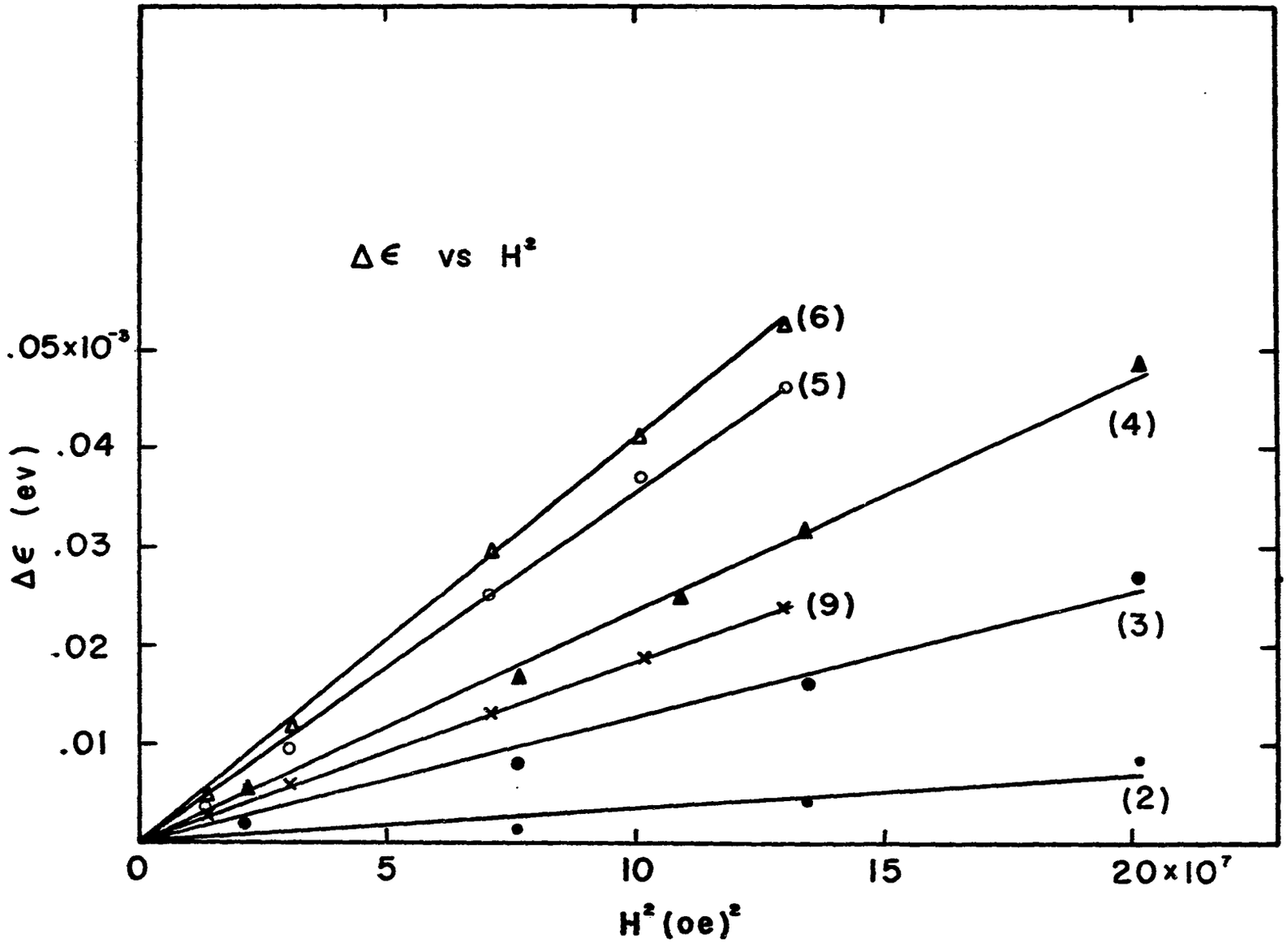

Fig. 3

TM_{110} MODE 5MM CAVITY AND COUPLING TO WAVEGUIDE

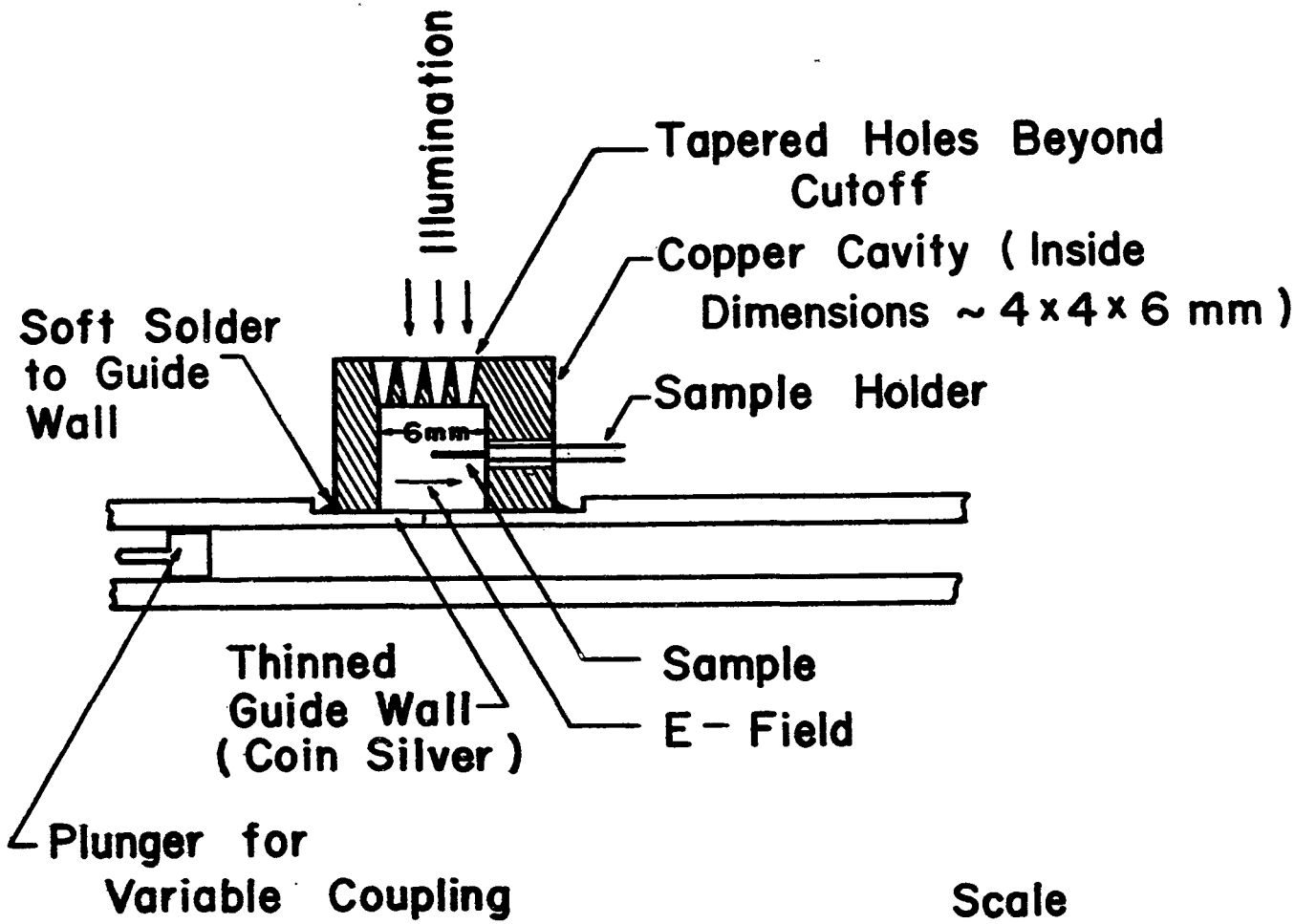

Scale ~ 1:4

Fig. 4

5MM CYCLOTRON RESONANCE APPARATUS

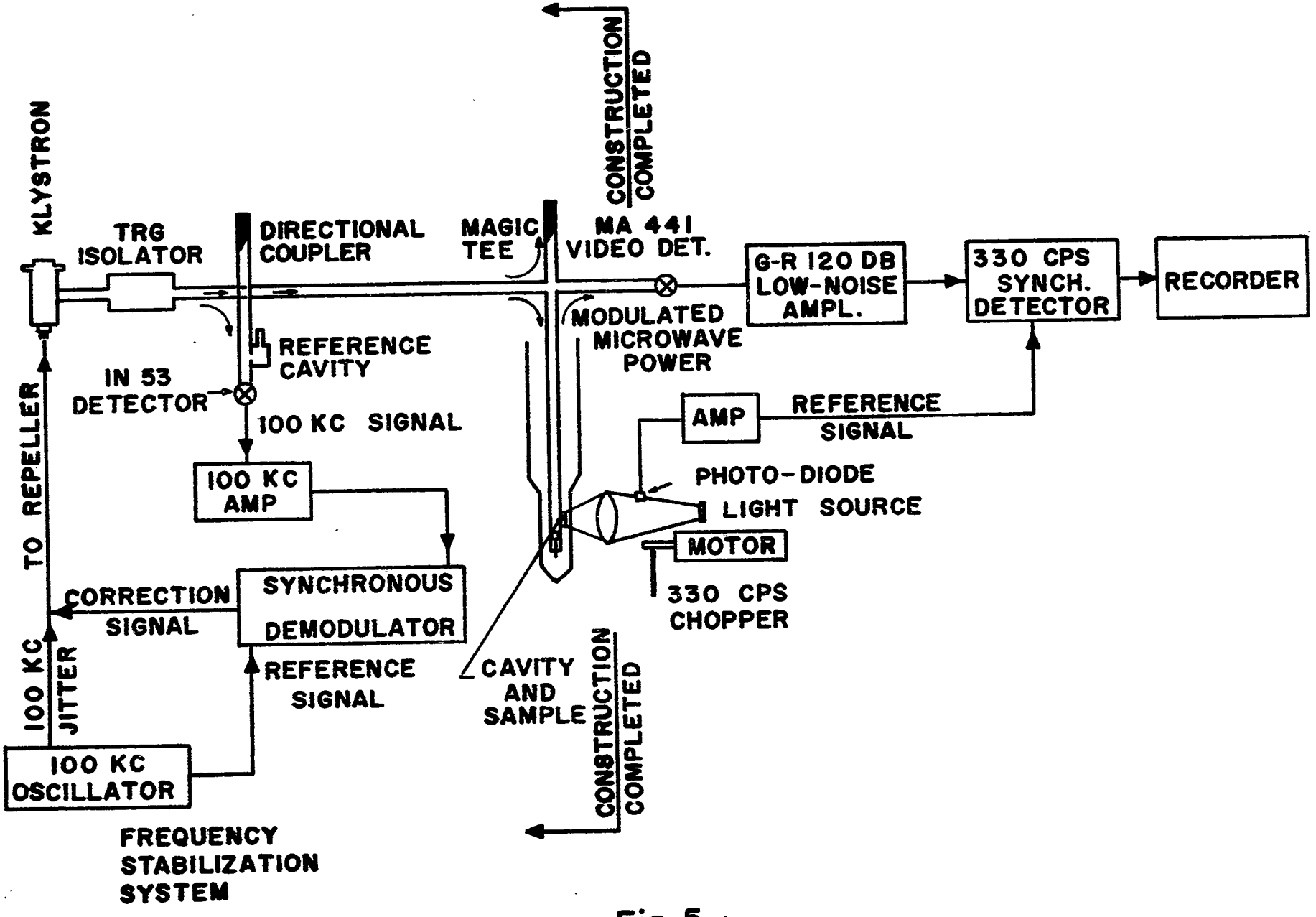

Fig. 5

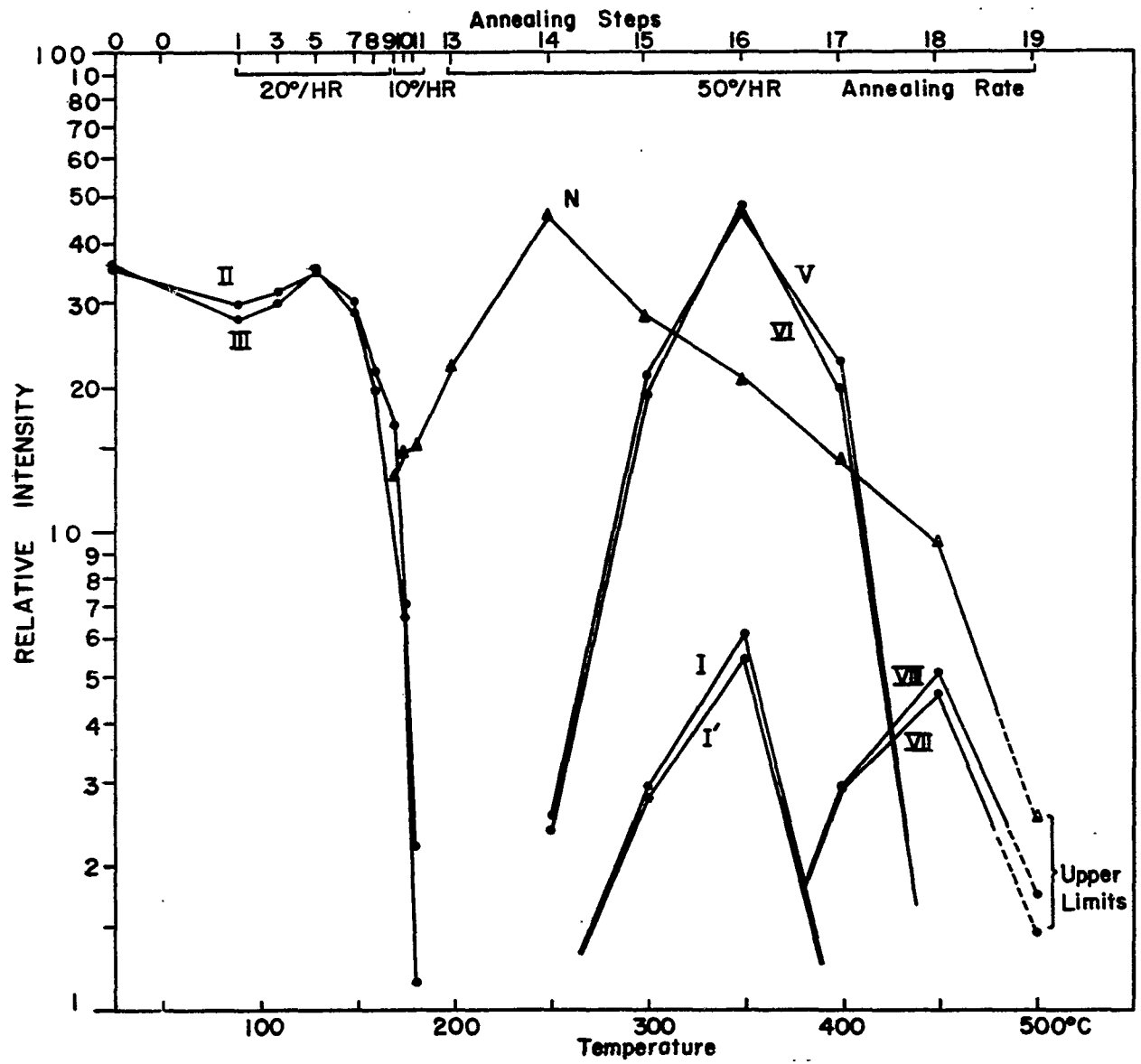

Isochronal Anneal of Neutron Irradiated Silicon Relative EPR Amplitudes vs. Temperature

US-SC #4, $\phi = 1.4 \times 10^{18}$ nvt (ORNL)

To Estimate Absolute Concentration, Multiply Scale by $1.24 \times 10^{13} (\Delta H)^2$

	$(\Delta H)^2$
II	1.44
III	1.44
N	1.44
V	1.44
VI	1.44
I	5.76
I'	5.76
VII	2.56
VIII	2.56

Fig. 6

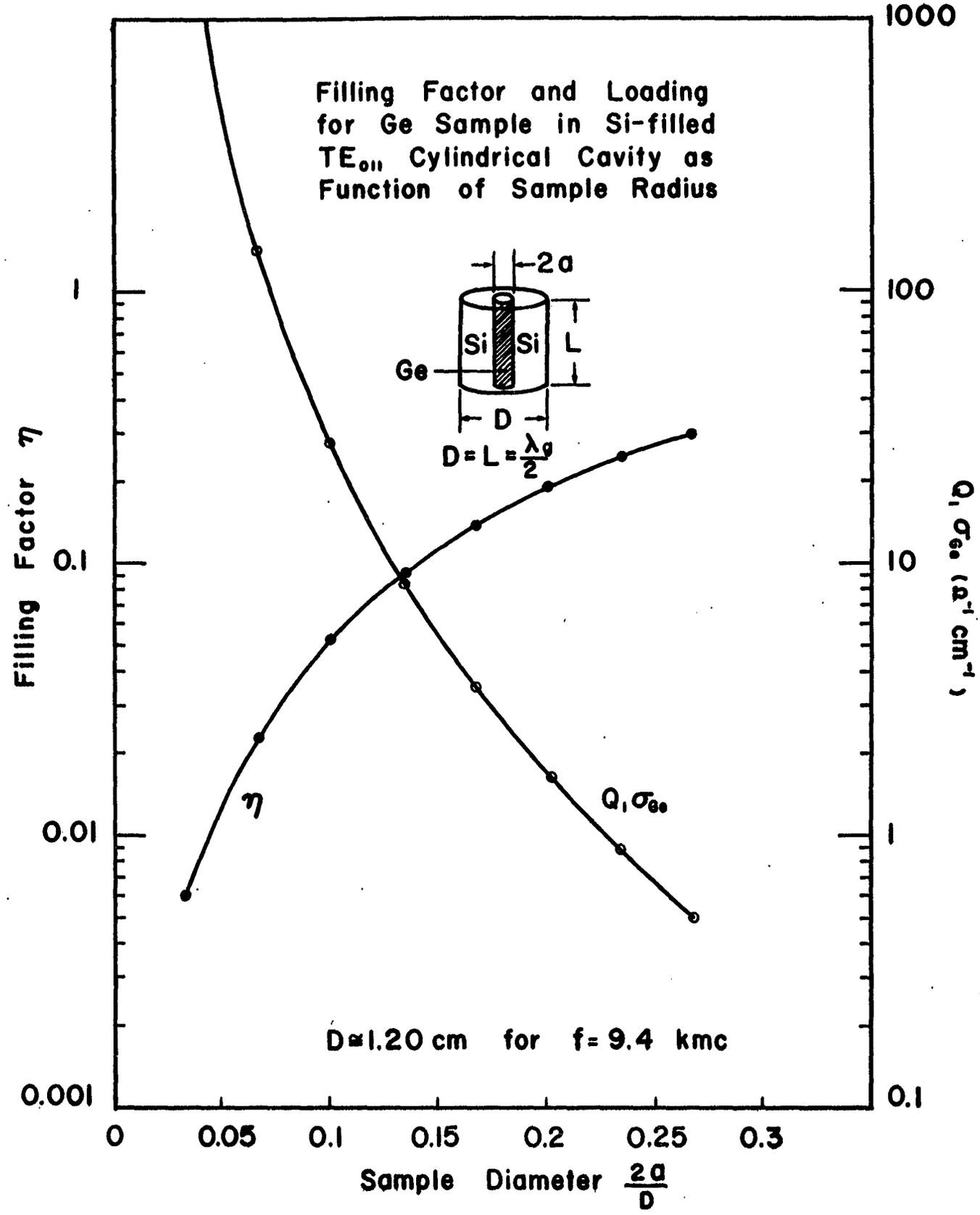
Filling Factor and Loading for Ge Sample in Si-filled TE_{011} Cylindrical Cavity as Function of Sample Radius
2a
Si
Si
Ge
L
D
$D = L = \frac{\lambda_g}{2}$
η
$Q_1 \sigma_{Ge}$
D≅1.20 cm for f= 9.4 kmc
Filling Factor η
$Q_1 \sigma_{Ge}$ (Ω^{-1} cm^{-1})
1000
100
10
1
0.1
1
0.1
0.01
0.001
0
0.05
0.1
0.15
0.2
0.25
0.3
Sample Diameter $\frac{2a}{D}$

Fig. 7

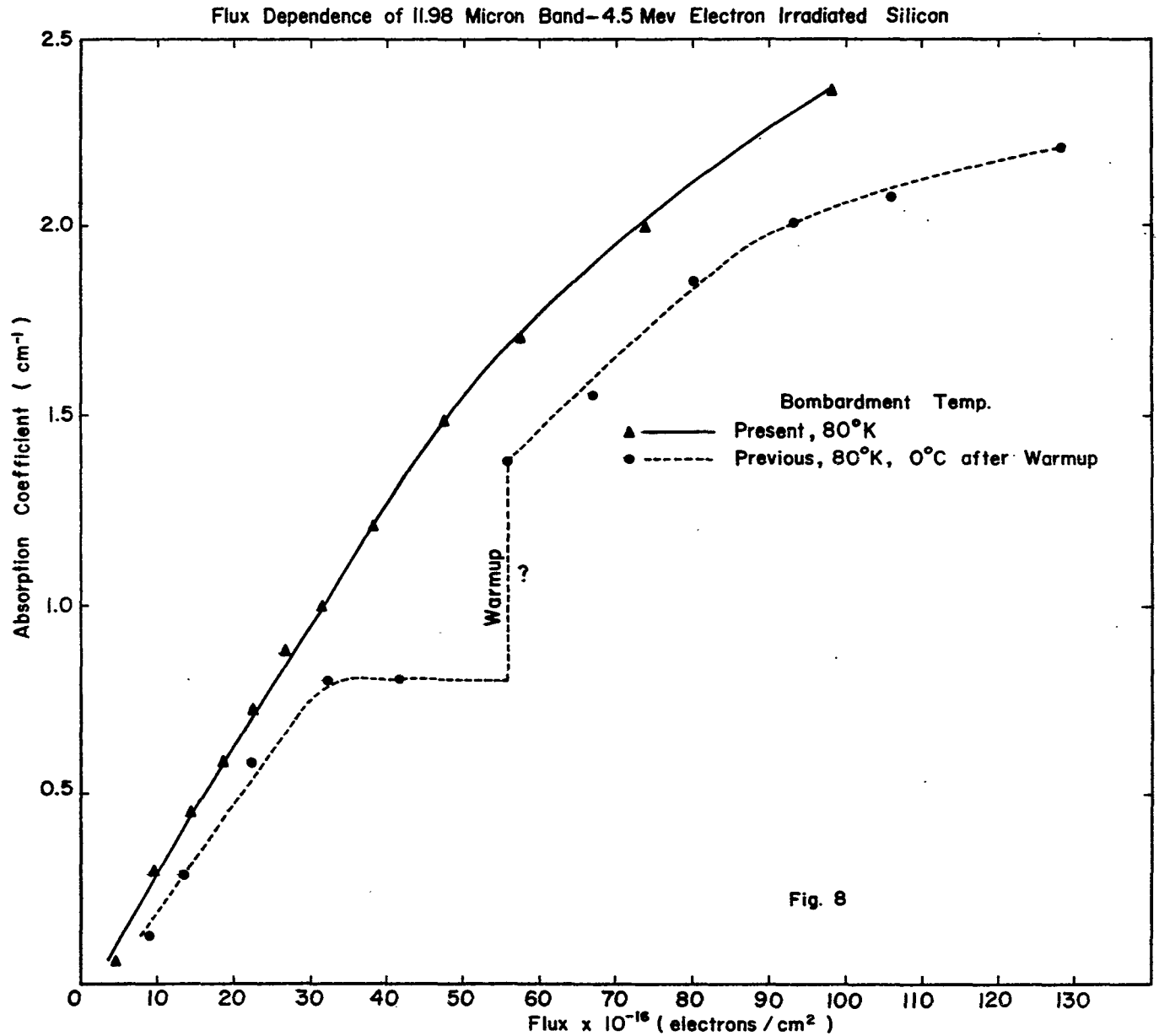
Flux Dependence of 11.98 Micron Band–4.5 Mev Electron Irradiated Silicon
Absorption Coefficient (cm⁻¹)
2.5
2.0
1.5
1.0
0.5
0
10
20
30
40
50
60
70
80
90
100
110
120
130
Flux x 10⁻¹⁶ (electrons / cm²)
Bombardment Temp.
Present, 80°K
Previous, 80°K, 0°C after Warmup
Warmup
?

Fig. 8

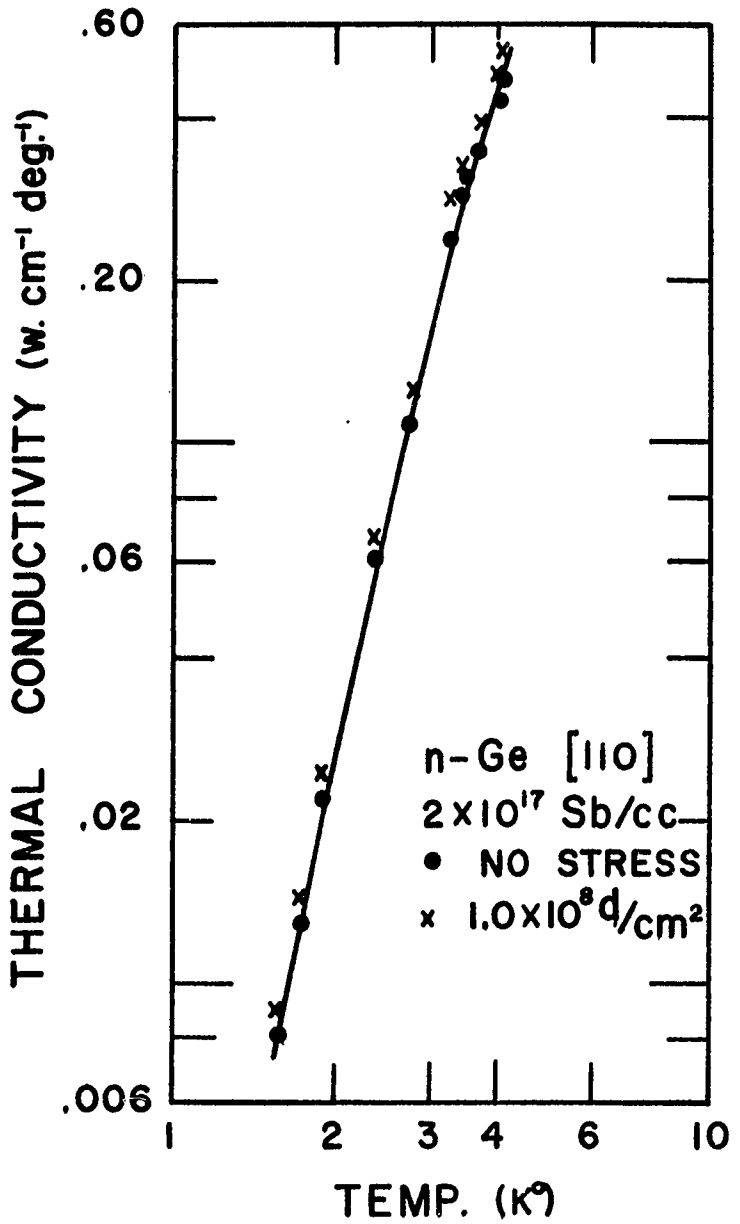
.60
.20
.06
.02
.006
THERMAL CONDUCTIVITY (w. cm⁻¹ deg⁻¹)
1
2
3
4
6
10
TEMP. (K°)
n-Ge [110]
2×10¹⁷ Sb/cc
• NO STRESS
× 1.0×10⁸ d/cm²

Fig. 9

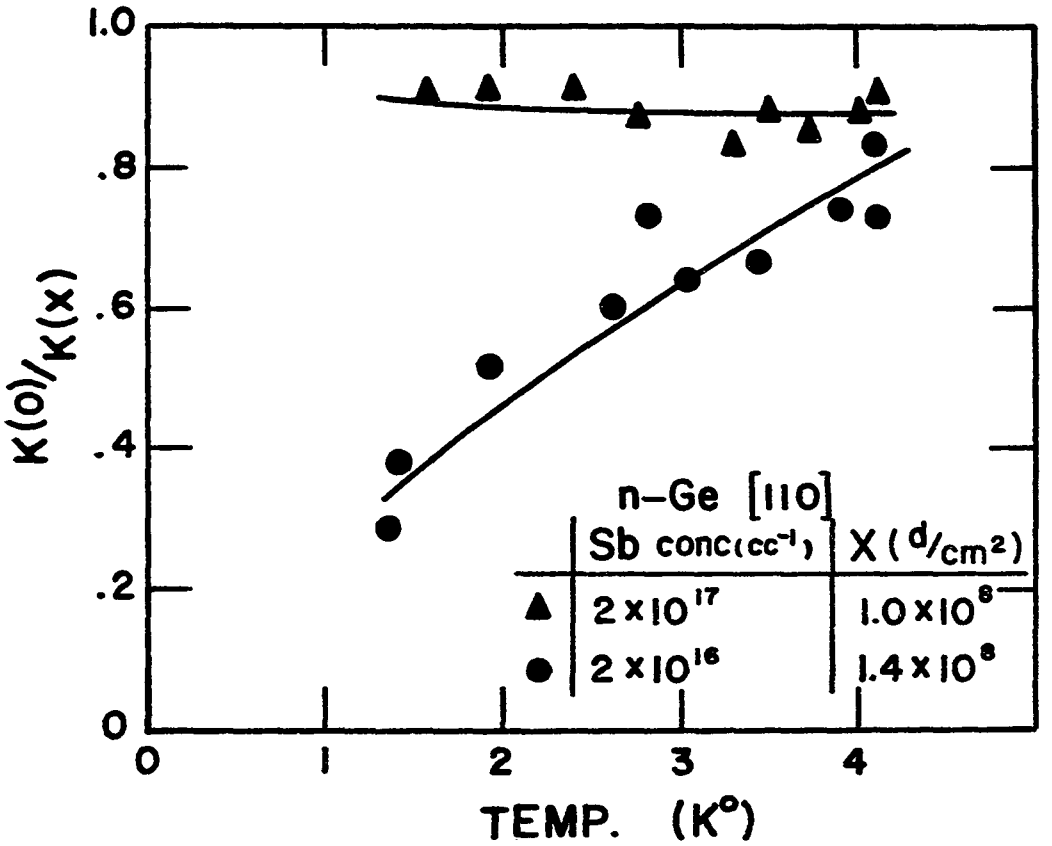
1.0
.8
.6
.4
.2
0
K(0)/K(x)
0
1
2
3
4
TEMP. (K°)
n–Ge [110]
Sb conc(cc⁻¹)
X (d/cm²)
2x10¹⁷
1.0x10⁸
2x10¹⁶
1.4x10⁸

Fig. 10

Ge THERMOMETER

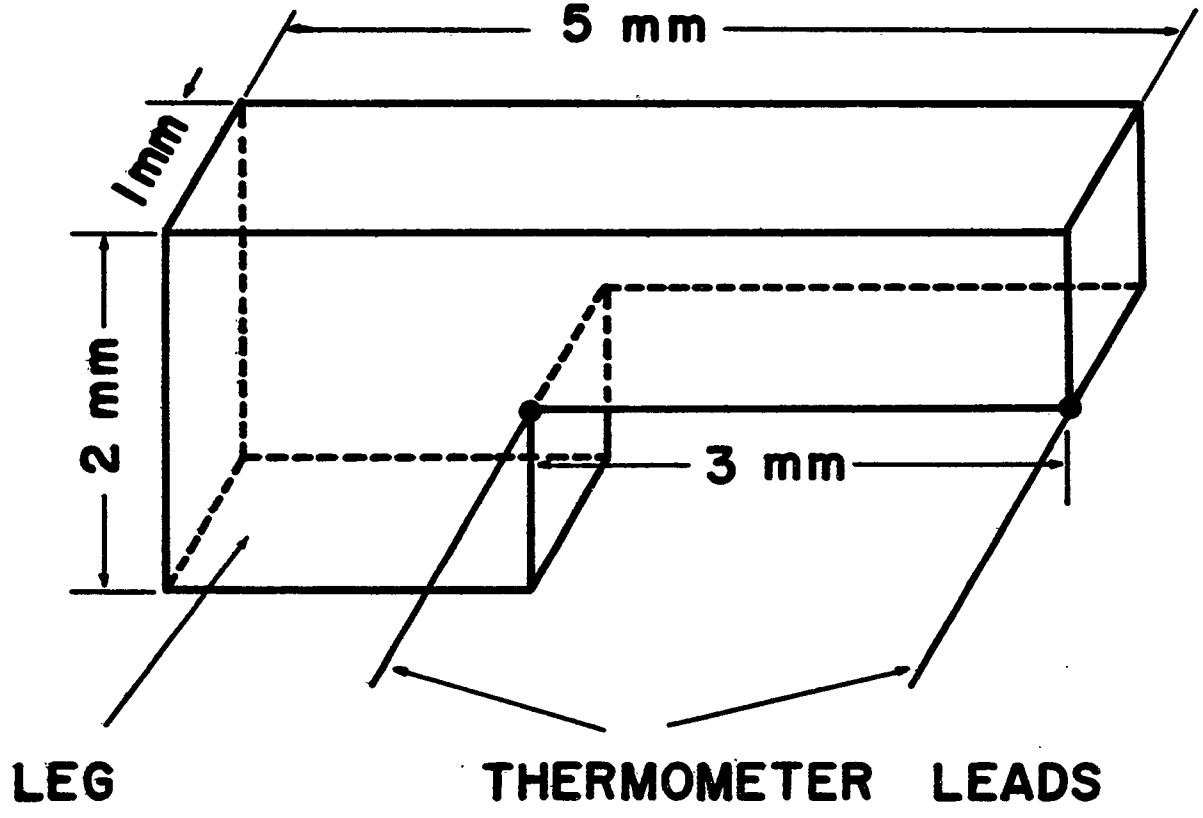

Fig. 11

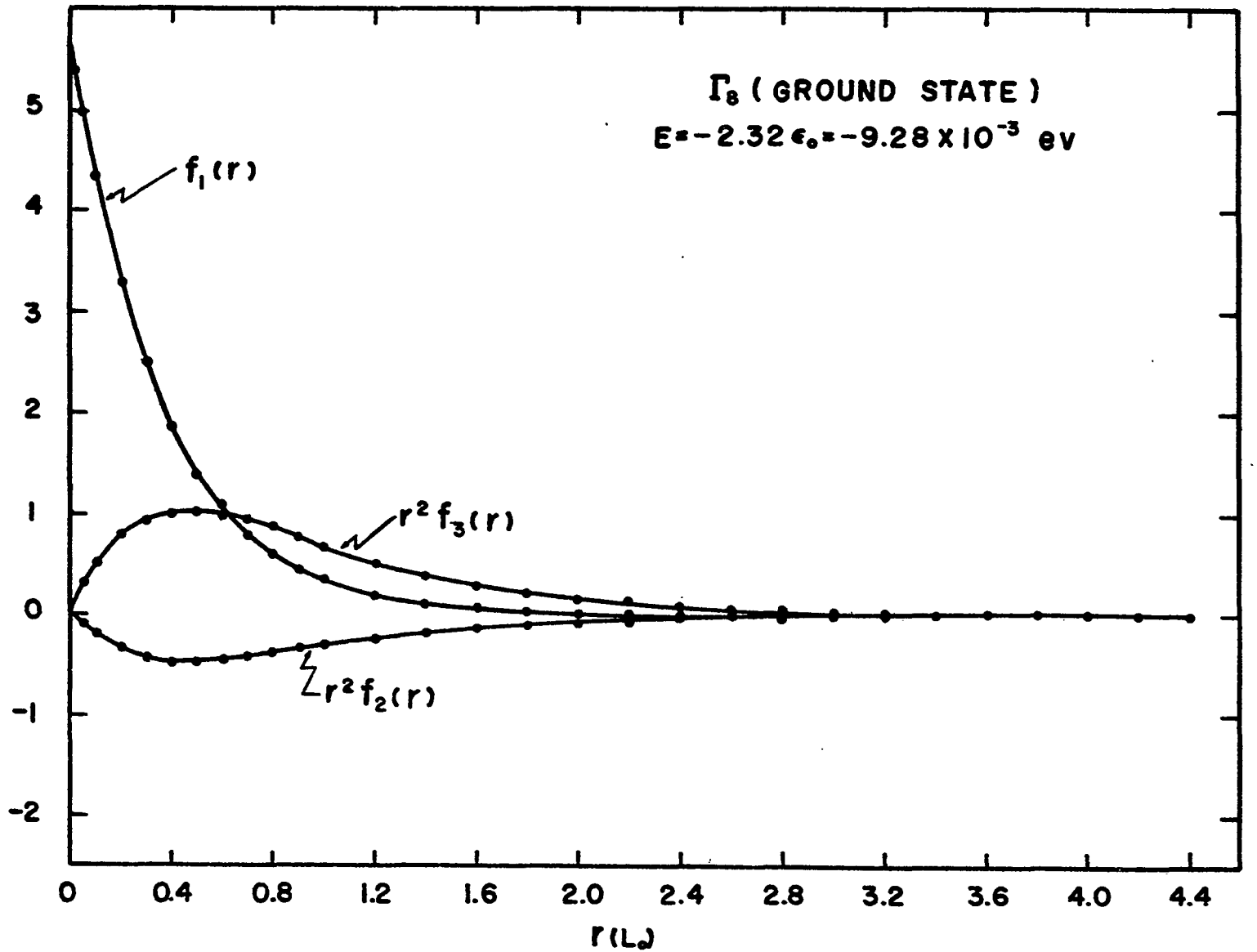
Γ_8 (GROUND STATE)
$E = -2.32\epsilon_0 = -9.28 \times 10^{-3}$ ev
$f_1(r)$
$r^2 f_3(r)$
$r^2 f_2(r)$
5
4
3
2
1
0
-1
-2
0
0.4
0.8
1.2
1.6
2.0
2.4
2.8
3.2
3.6
4.0
4.4
r(L.)

Fig. 12

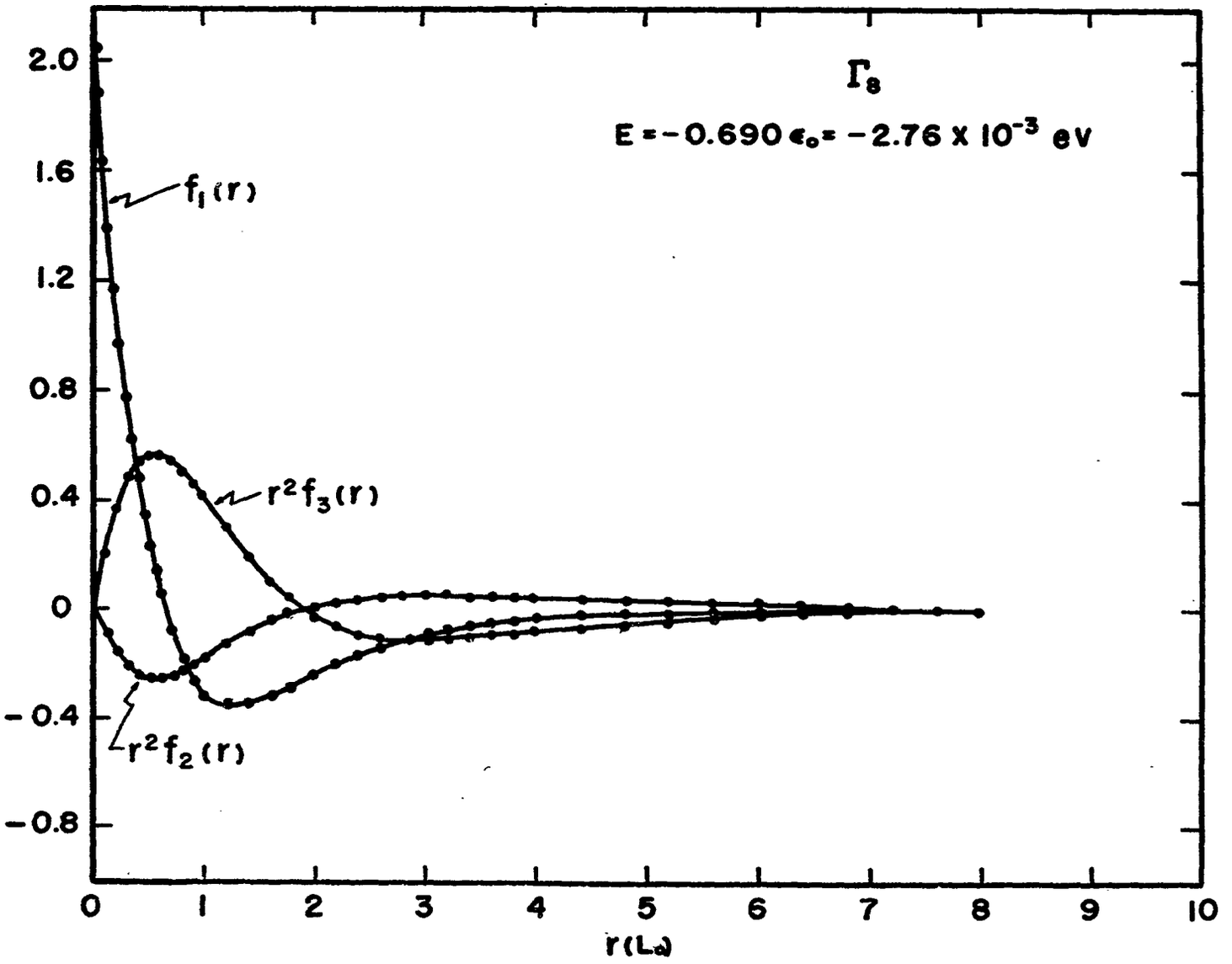
Γ_8
E = −0.690 ϵ_o = −2.76 x 10^{-3} eV
$f_1(r)$
$r^2 f_3(r)$
$r^2 f_2(r)$
2.0
1.6
1.2
0.8
0.4
0
−0.4
−0.8
0
1
2
3
4
5
6
7
8
9
10
r(La)

Fig. 13

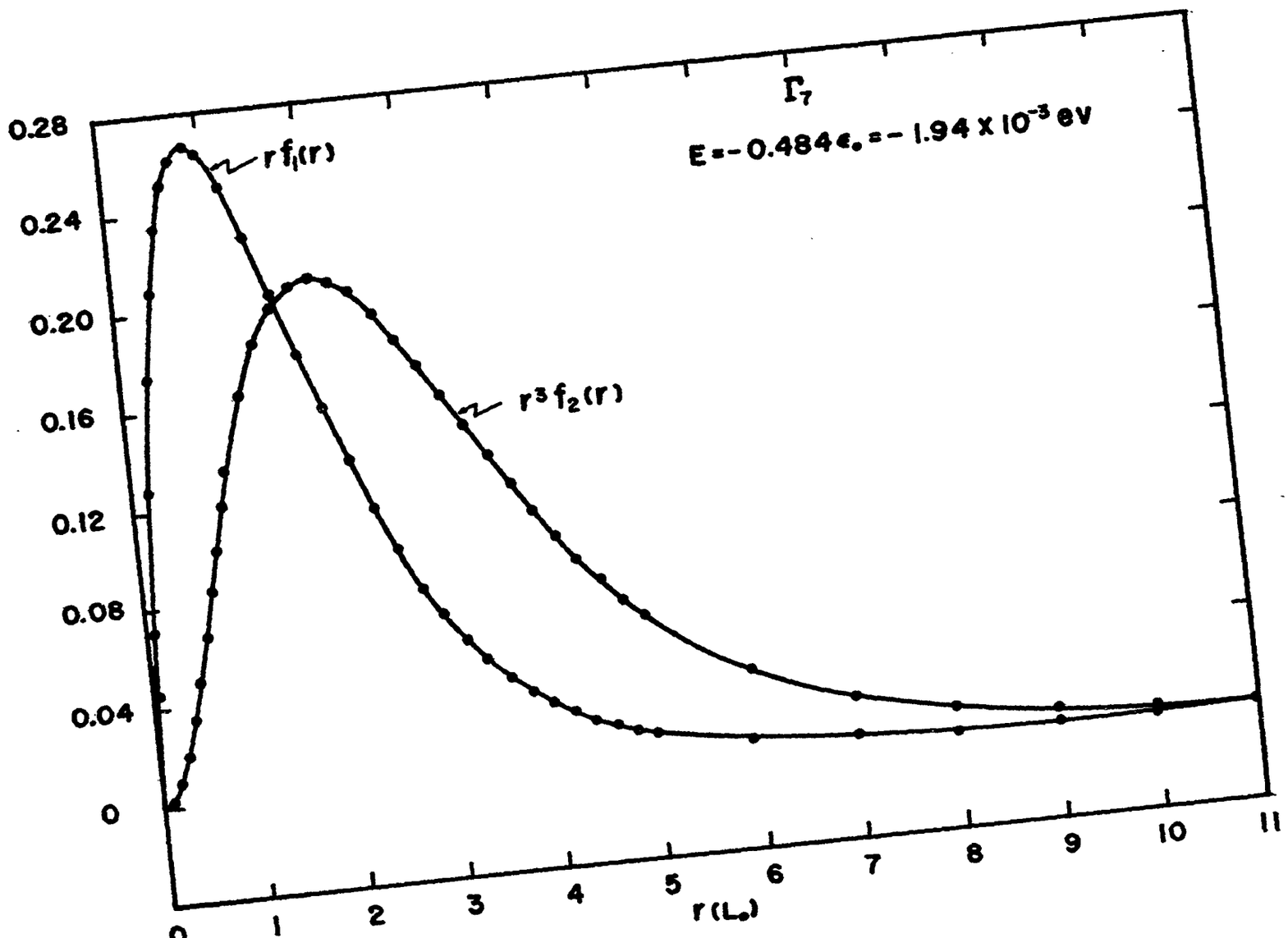
Γ_7
$E = -0.484\epsilon_0 = -1.94 \times 10^{-3}$ eV
$r f_1(r)$
$r^3 f_2(r)$
0.28
0.24
0.20
0.16
0.12
0.08
0.04
0
0
1
2
3
4
5
6
7
8
9
10
11
$r(L_0)$

Fig. 14

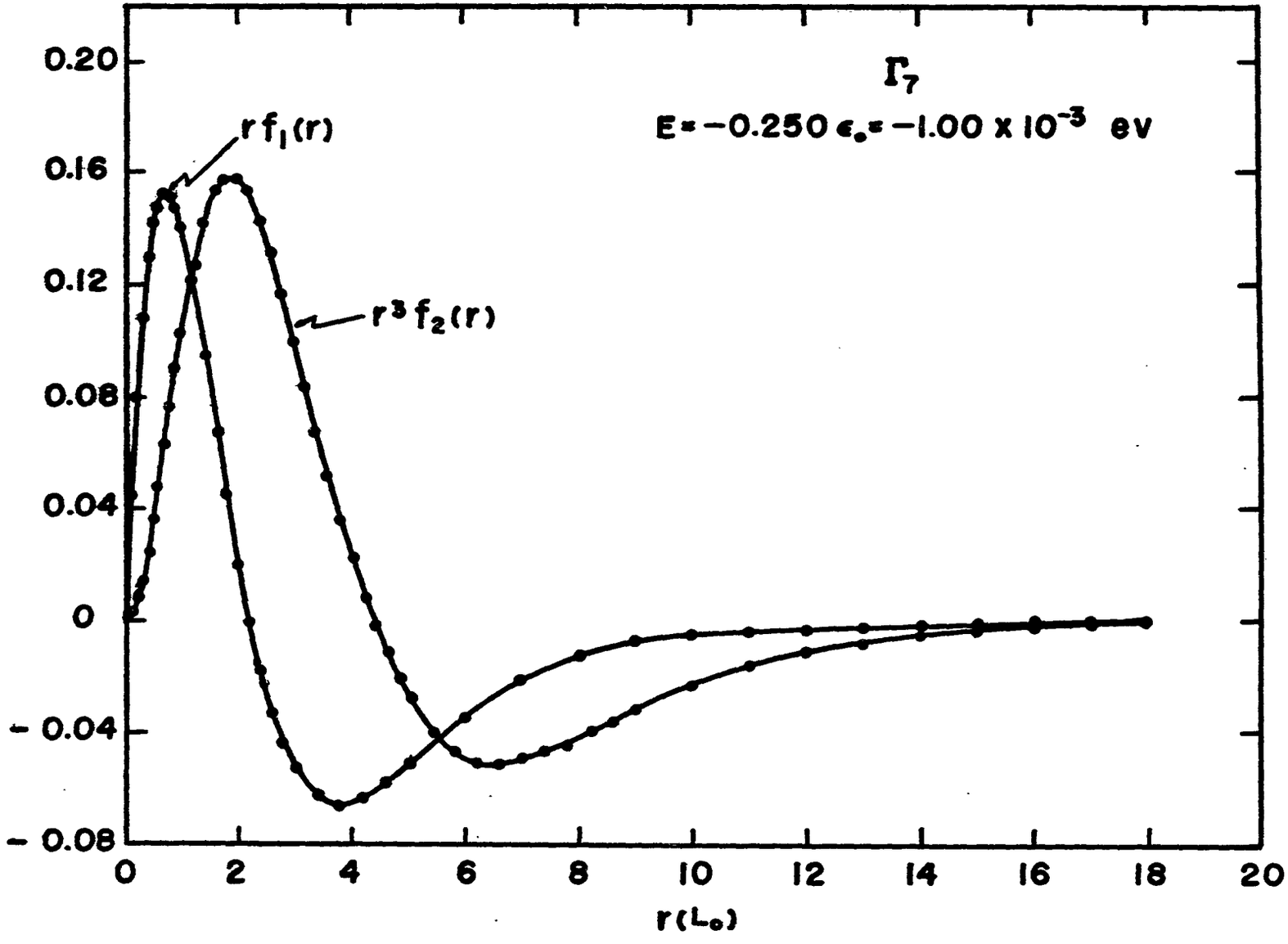
0.20
0.16
0.12
0.08
0.04
0
- 0.04
- 0.08
0
2
4
6
8
10
12
14
16
18
20
r(L₀)
Γ₇
E = −0.250 ε₀ = −1.00 x 10⁻³ ev
r f₁(r)
r³ f₂(r)

Fig. 15

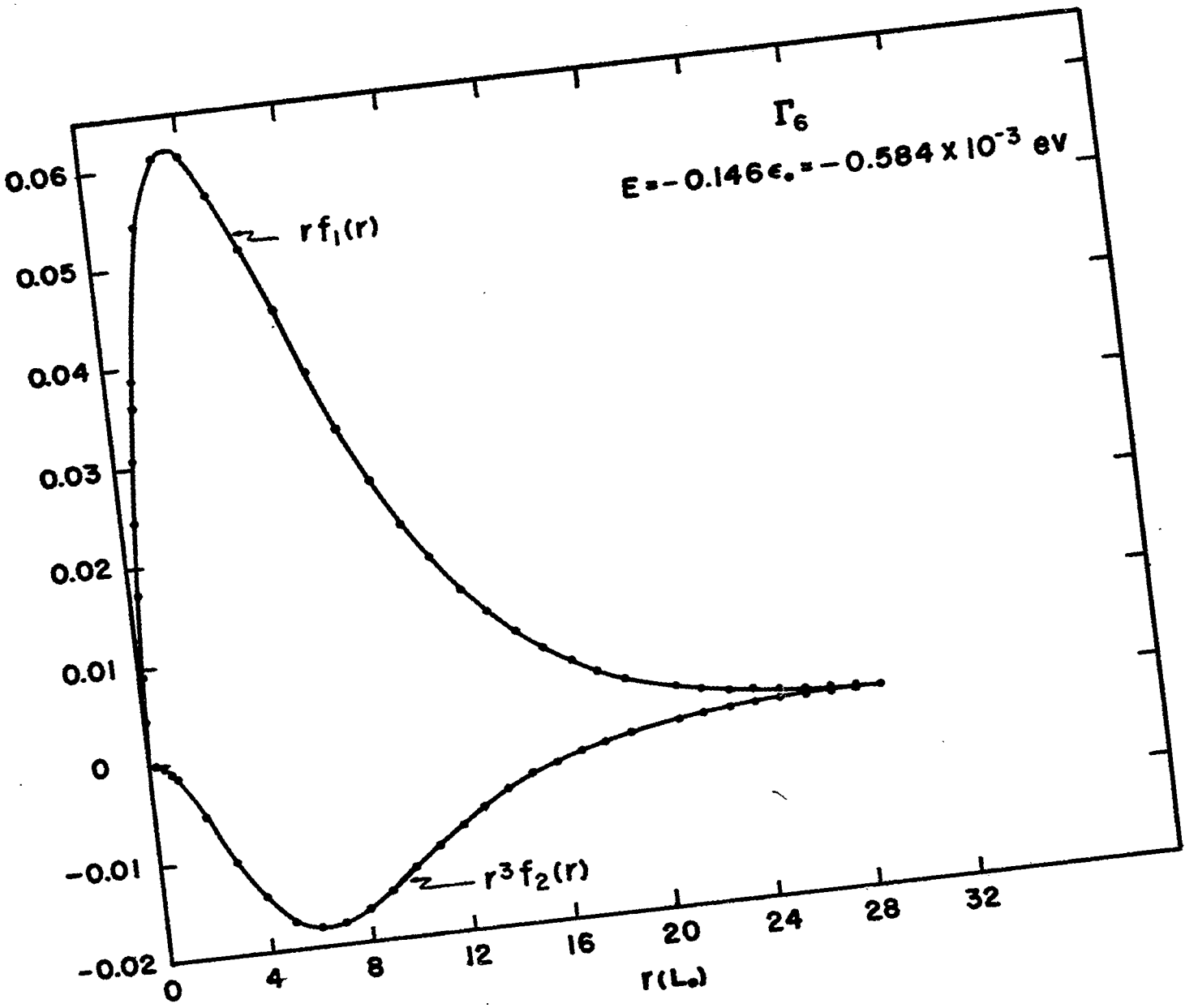
Γ_6
$E = -0.146\epsilon_0 = -0.584 \times 10^{-3}$ eV
$rf_1(r)$
$r^3 f_2(r)$
0.06
0.05
0.04
0.03
0.02
0.01
0
-0.01
-0.02
0
4
8
12
16
20
24
28
32
$r(L_0)$

Fig. 16

Distribution List

	No. of Copies
Director National Bureau of Standards Boulder, Colorado Attn: Radio Library	1
Commander, Air Force Command and Control Development Division Air Research and Development Command U. S. Air Force L. G. Hanscom Field Bedford, Massachusetts Attn: CROTR 2E	1
Director U. S. Naval Research Laboratory Washington 25, D. C. Attn: Code 2027	1
Chief Signal Officer Department of the Army Washington 25, D. C. Attn: SIGRD	1
Commander Armed Services Technical Information Agency Arlington Hall Station Arlington 12, Virginia	10
Commander Wright Air Development Division Wright-Patterson Air Force Base, Ohio Attn: WCOSI-3 Attn: WCLKT-4	1 1
Department of the Navy Bureau of Ships Semiconductor Unit, Code 691A Washington 25, D. C. Attn: Mr. A. H. Young	1
Chief, Bureau of Ships Department of the Navy Washington 25, D. C. Attn: Code 327	1
Office of Naval Research Department of the Navy Washington 25, D. C. Attn: Code 427	1

DA36-039 sc-87394

	No. of Copies
Director U. S. Naval Research Laboratory Washington 25, D. C. Attn: Code 3560	1
Advisory Group on Electron Devices 346 Broadway New York 13, New York	2
Commanding Officer Watertown Arsenal Watertown, Massachusetts Attn: ORDO	1
Commander Air Research and Development Command Andrews Air Force Base Washington 25, D. C. Attn: RDRR-2	1
Commanding Officer U. S. Army Signal Electronics Research Unit Mountain View, California	1
Commandant Anti-aircraft Artillery and Guided Missile School Fort Bliss, Texas	1
U. S. Naval Inspector of Ordnance Applied Physics Laboratory Johns Hopkins University Silver Spring, Maryland	1
Atomic Energy Commission Metallurgy Branch Division of Research Washington 25, D. C. Attn: Mr. J. F. White	1
New York Naval Shipyard Brooklyn 1, New York Attn:; Material Laboratory, Code 912b	1
Naval Ordnance Laboratory Silver Spring, Maryland Attn: Solid State Division	1
Director, U. S. Naval Research Laboratory Washington 25, D. C. Attn: Code 6451	1

DA36-039 sc-87394 — No. of Copies

Commanding Officer and Director
U. S. Naval Electronics Laboratory
San Diego 52, California — 1

Technical Library
OASD (R and E)
Rm 3E1065, The Pentagon
Washington 25, D. C. — 1

Chief of Ordnance
Washington 25, D. C.
Attn: ORDTX-AR — 1

Commanding General
U. S. Army Ordnance Missile Command
Redstone Arsenal, Alabama
Attn: ORDXM-DR — 1

Commanding Officer
Frankford Arsenal
Philadelphia 37, Pennsylvania
Attn: ORDBA-FEL — 1

Commander
Rome Air Development Center
Griffiss Air Force Base, New York
Attn: RCSST-3 — 1

Commanding Officer
Diamond Ordnance Fuze Laboratory
Connecticut Avenue and Van Ness Street
Washington 25, D. C.
Attn: T. T. Liimatainen — 1

Commanding Officer
U. S. Army Signal Equipment Support Agency
Fort Monmouth, N. J.
Attn: SIGFM/ES-ASA — 1

Army Liaison Office
U. S. Naval Research Laboratory
Washington 25, D. C. — 1

Commander
Rome Air Development Center
Griffiss Air Force Base, New York
Attn: RCRWE-3 — 1

Chief of Ordnance
Washington 25, D. C.
Attn: ORDTB-Materials — 1

DA36-039 sc-87394 — No. of Copies

Continental Army Command Liaison Office
U. S. Army Signal Research and Development Laboratory
Fort Monmouth, New Jersey — 1

U. S. Office of Naval Research
National Bureau of Standards
Corona, California — 1

Commanding Officer
U. S. Army Signal Research and Development Laboratory
Fort Monmouth, New Jersey
Attn: Technical Information Division — 1
FOR RETRANSMITTAL TO: Canadian Liaison Officer
Office of the Chief Signal Officer
Room 2B274, Pentagon
Washington 25, D. C.

Commanding Officer
Engineering Research and Development Laboratories
Fort Belvoir, Virginia
Attn: Technical Intelligence Branch — 1

Battelle Memorial Institute
505 King Avenue
Columbus 1, Ohio
Attn: A. C. Beer — 1

Chicago Midway Laboratories
University of Chicago
Chicago 37, Illinois
Attn: Librarian — 1

Technical Reports Collection
303A Pierce Hall
Harvard University
Cambridge 38, Massachusetts
Attn: Librarian — 1

Franklin Institute
20th Street and Benjamin Parkway
Philadelphia, Pennsylvania — 1

University of Illinois
Urbana, Illinois
Attn: Dr. J. Bardeen — 1

Westinghouse Electric Corporation
Youngwood, Pennsylvania
Attn: R. K. Riel — 1

DA36-039 sc-87394 — No. of Copies

Northwestern University
Evanston, Illinois
Attn: Dr. W. Nuxford — 1

Chief of Research and Development
OCS, Department of the Army
Washington 25, D. C. — 1

Hughes Aircraft Company
Semiconductor Division
P. O. Box 278
Newport Beach, California
Attn: Library — 1

National Bureau of Standards
U. S. Department of Commerce
Washington 25, D. C.
Attn: P. J. Solgin — 1

Philco Corporation
"C" and Tioga Streets
Philadelphia, Pennsylvania
Attn: Mr. W. H. Forster — 1

General Electric Company
Semiconductor Products Department
Electronics Park
Syracuse, New York
Attn: Dr. H. M. Sullivan, Advanced Semiconductor Lab. — 1

Raytheon Company
150 California Street
Newton, Massachusetts
Attn: Mr. H. L. Gaudreau, Administrator
Government Contracts — 1

Bell Telephone Laboratories
Murray Hill, New Jersey
Attn: Mr. A. Anderson — 1

Radio Corporation of America
Harrison, New Jersey
Attn: C. M. Bost — 1

Brown University
Providence 12, Rhode Island — 1

Massachusetts Institute of Technology
P. O. Box 73
Lexington 73, Massachusetts
Attn: Library A-229 — 1

DA36-039 sc-87394

No. of Copies

University of Minnesota
Institute of Technology
Minneapolis 14, Minnesota
Attn: Dr. A. van der Ziel — 1

New York University
College of Engineering
University Heights
New York 53, New York
Attn: Dr. I. Cadoff — 1

Massachusetts Institute of Technology
Research and Development Laboratories
Cambridge 39, Massachusetts
Attn: Documents Office, Room 20B-221 — 1

Notre Dame University
Physics Department
South Bend, Indiana
Attn: Prof. J. C. Buch — 1

University of Michigan
Willow Run Research Center
Ypsilanti, Michigan
Attn: Librarian, IRIA — 1

Pennsylvania State University
College of Engineering and Architecture
University Park, Pennsylvania
Attn: S. H. Chamberlain, Librarian — 1

Sanders Associates, Inc.
Nashua, New Hampshire — 1

North American Aviation
International Airport
Los Angeles, California — 1

National Carbon Company
Division of Union Carbide Corporation
P. O. Box 6116
Cleveland, Ohio
Attn: Library — 1

Mr. Robert K. Willardson, Assistant Chief
Physical Chemistry Division
Battelle Memorial Institute
505 King Avenue
Columbus 1, Ohio — 1

DA36-039 sc-87394 — No. of Copies

Honeywell Research Center
500 Washington Avenue, South
Hopkins, Minnesota
Attn: Dr. Van W. Bearinger — 1

Semiconductor Components Library
Texas Instruments, Inc.
P. O. Box 5012
Dallas 22, Texas — 1

Stanford University
Palo Alto, California
Attn: Dr. John Moll, Electrical Engineering Department — 1

Commander
U. S. Naval Ordnance Test Station
China Lake, California
Attn: Code 5019 — 1

International Rectifier Corporation
1521 East Grand Avenue
El Segundo, California
Attn: Dr. C. A. Escoffery — 1

Chief, U. S. Army Security Agency
Arlington Hall Station
Arlington 12, Virginia — 2

Commanding Officer
U. S. Army Research Office (Durham)
Attn: CRD-AA-IP, Mr. Ulsh
Box CH, Duke Station
Durham, N. Carolina — 3

Commanding Officer
U. S. Army Signal Research and Development Laboratory
Fort Monmouth, New Jersey
Attn: Director of Research — 1
Attn: Chief, Technical Documents Center — 1
Attn: Chief, Technical Information Division — 3
Attn: Exploratory Research Division "E" — 1
Attn: Microwave Quantum and Electronics Br, Solid State and Frequency Control Div — 1
Attn: Mr. P. Newman, Solid State and Frequency Control Div — 3

Deputy President
U. S. Army Security Agency Board
Arlington Hall Station
Arlington 12, Virginia — 1

DA36-039 sc-87394

No. of Copies

Sylvania Electric Products, Inc.
Semiconductor Division
100 Sylvan Road
Woburn, Massachusetts
Attn: Mr. F. H. Bower — 1

Diamond Ordnance Fuze Laboratories
U. S. Army Ordnance Corps
Attn: ORD and L - 450-638
Mr. Raymond H. Comyn
Washington 25, D. C. — 1

Total number of copies to be distributed — ~ 100

This contract is supervised by the Institute for Exploratory Research, USASRDL, Fort Monmouth, N. J..

Scientific contact at Purdue: Dr. H. Y. Fan
Scientific contact at Signal R and D Laboratory: Dr. S. Benedict Levin
Telephone 201-535-1308